COMPUTER AIDED DESIGN OF NOVEL NOSCAPINOIDS AND THEIR EXPERIMENTAL EVALUATION AS TUBULIN BINDING ANTI-CANCER DRUGS

BY

SENEHA SANTOSHI
Enrollment No. 106501

SYNOPSIS

OF THE THESIS SUBMITTED IN FULFILLMENT OF THE REQUIREMENTS FOR

THE DEGREE OF DOCTOR OF PHILOSOPHY
IN
BIOINFORMATICS

UNDER THE GUIDANCE OF
DR. PRADEEP KUMAR NAIK

DEPARTMENT OF BIOTECHNOLOGY & BIOINFORMATICS
JAYPEE UNIVERSITY OF INFORMATION TECHNOLOGY
WAKNAGHAT, SOLAN-173234, HP, INDIA

MAY 2014

COMPUTER AIDED DESIGN OF NOVEL NOSCAPINOIDS AND THEIR EXPERIMENTAL EVALUATION AS TUBULIN BINDING ANTI-CANCER DRUGS

SENEHA SANTOSHI

INTRODUCTION

Cancer is one of the leading causes of death. According to the latest report released in December 2013 by International Agency for Research on Cancer (IARC), the specialized cancer agency of the World Health Organization, global burden of cancer rises to 14.1 million new cases and 8.2 million deaths in 2012. In the context of India, cancer is the second most common disease responsible for maximum mortality with about 0.3 million deaths per year [1]. Among all the treatment regimens, chemotherapy is widely used for treatment and prevention of reoccurrence for a variety of cancer types. Along with DNA binding drugs, microtubules (MT) interacting drugs are now included in the first-line therapeutic modalities in many types of cancers. This is because microtubules are major cytoskeleton structures of cells and are responsible for maintaining the cell shape, physiological activity and cell division of cells.

The dynamics of microtubule polymers which can be described as their growth rate at the plus ends, catastrophic shortening, frequency of transition between the two phases, pause between the two phases, their release from the microtubule organizing center and treadmilling [2-4] is absolutely crucial for the cellular activities. Interference with microtubules dynamics often leads to programmed cell death and thus microtubule-binding drugs such as paclitaxel, docetaxel and the vinca alkaloids are currently used to treat various malignancies in the clinic. However, these chemotherapy drugs are confounded by complications with serious toxicity (particularly, peripheral neuropathies, gastrointestinal toxicity, myelosuppression and immunosuppression) owing to their non-selective action and extreme overpolymerizing effects (by taxanes) or depolymerizing effects (by vincas) on microtubules [5-9]. Thus, there is an urgent need to explore novel tubulin-binding agents that are significantly effective and comparatively less toxic compared to currently-available drugs for the treatment of human cancers. Systematic screening of new compounds based on structural similarity of known drugs (such as colchicine, podophyllotoxin, etc.) that interfere with microtubules, Noscapine (an opium alkaloid) was discovered that binds stoichiometrically to tubulin, alters its conformation upon binding and arrests mammalian cells in mitosis [10]. It was demonstrated that unlike many other microtubule inhibitors, Noscapine does not significantly promote or inhibit microtubule polymer mass even at high concentrations. Instead, it alters the steady-state dynamics of microtubule assembly, primarily by increasing the amount of time that the

microtubules spend in an attenuated (pause) state when neither microtubule growth nor shortening is detectable [11] (Figure 1). Noscapine-induced suppression of microtubule dynamics, even though subtle, is sufficient to interfere with the proper attachment of chromosomes to kinetochore microtubules and to suppress the tension across paired kinetochores [13]. Noscapine thus effectively inhibits the progression of various cancer types both in cultured cells and in animal models with no obvious side effects to the kidney, heart, liver, bone marrow, spleen, or small intestine, and does not inhibit primary humoral immune responses in mice [10,11,14]. Surprisingly, the apoptosis is much more pronounced in cancer cells compared with normal healthy cells [11]. In addition, Noscapine has some other advantage properties as lead molecule: (1) retains activity against paclitaxel-resistant cell lines (1A9/PTX10, 1A9/PTX22) and epothilone-resistant cell line (1A9/A8) [12]; (2) a favourable pharmacokinetics (clearance in 6-10 hours); (3) a poor substrate for drug-pumps (polyglycoproteins and MDR-related proteins) [15] that comprise a major cause of drug resistance; (4) it does not show immunological [16] and neurological toxicities [17]. Although Noscapine is cytotoxic in a variety of different cancer cell lines (NCI 60 cell lines panel), the IC_{50} values remain in the high micromolar ranges (~21.1 to 100 μM). Also it inhibits tumorigenesis *in vivo* albeit at high concentrations (~ 300 mg/kg body weight) [18,19]. To enhance its activity further an array of Noscapine derivatives (collectively called as Noscapinoids) were developed which are at different stages of chemical and biological characterization. It is noteworthy that Noscapinoids cause no histopathological, hematological, immunological and neuronal toxicity at concentrations as high as 300 mg/kg [10,12,13,18,19]. These Noscapine derivatives inhibit cellular proliferation of a wide variety of cancer cells (panel of NCI 60 cancer cell lines) including many drug-resistant variants while evading normal cells. In addition they effectively regress human tumor xenografts (lymphomas, breast, prostate and melanomas) implanted in preclinical mice models to a fair degree. However, a complete elimination of the disease was not achieved even on increasing dosages as high as 600 mg/kg. Therefore attempts should be made to design new generation of Noscapine derivatives for the better therapeutic outcome.

Availability of structure activity data of many derivatives of Noscapine leads to develop a reasonable prediction model and thus guided in rational design of more potent derivatives of Noscapine. Furthermore, chemical synthesis and experimental evaluation of newly designed potent Noscapinoids indicate a great potential as chemotherapeutic agent for the treatment of human cancers to treat various malignancies in the clinic.

(A)

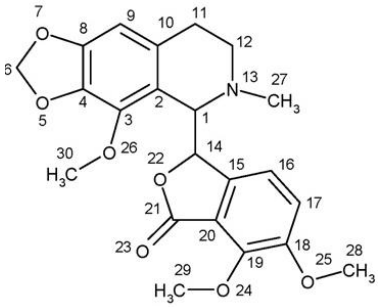

(B)

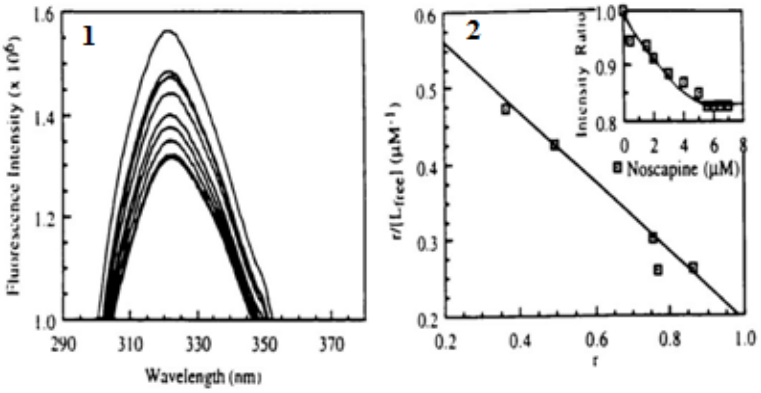

(C)

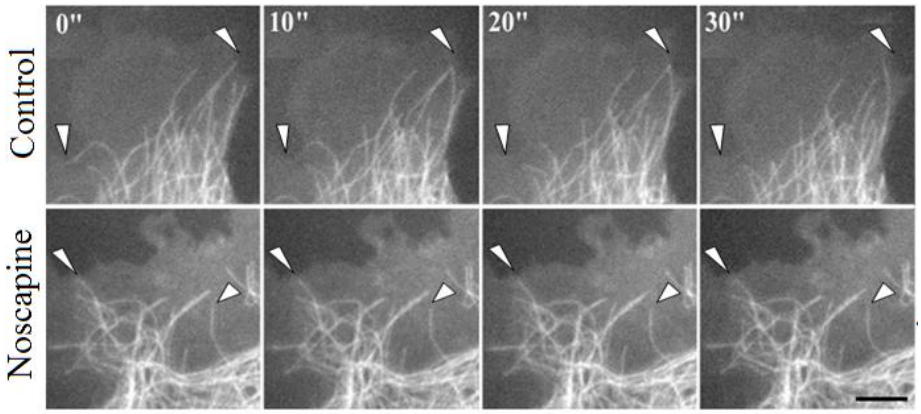

(D)

Dynamic Parameters	Control	Noscapine 25μM	Noscapine 250μm
Growth	37 MTs n=96	45 MTs n=89	44 MTs n=14
Rate (μm/min)	9.89 ±0.78	9.29 ±1.05	6.34 ±0.72
Distance (mm)	1.16 ±0.09	0.97 ±0.10	0.75 ±0.03*
Duration (sec)	9.62 ±0.95	8.30 ±1.44	8.04 ±0.74
Shrink	n=78	n=79	n=19
Rate (μm/min)	11.39 ±0.81	9.06 ±0.76*	8.89 ±1.19*
Distance (mm)	1.60 ±0.30	1.04 ±0.09	1.26 ±0.36
Duration (sec)	8.75 ±1.26	8.06 ±0.58	9.62 ±2.13
Average Pause Duration (sec)	n=109 22.54 ±2.18	n=132 34.66 ±3.27*	n=68 77.60 ±5.68*
% Time per Phase Growth/Shrink/Pause	22.7/16.8/60.5	12.3/10.8/76.9	2.0/3.3/94.7
Rescue Frequency (sec^{-1})	0.147 ±0.02	0.128 ±0.01	0.138 ±0.03
Catastrophe Frequency (sec^{-1})	0.029 ±0.004	0.028 ±0.004	0.007 ±0.001*
Dynamicity (μm/min)	102.70 ±12.94	57.50±7.72*	10.40 ±2.83*

Figure 1. Noscapine as tubulin binding agent. (A) The molecular structure of Noscapine with numbering of atoms. (B.1) Titration of fluorescence spectra of tubulin at different concentration of Noscapine. (B.2) Scatchard plot showing an apparent dissociation constant (K_d) of 144 ± 1.0 μM. (C) Noscapine increases the average time cellular microtubules remain inactive (pause duration). A gallery of video frames, 10 seconds apart, showing the plus ends of several microtubules in a control and Noscapine-treated cells. (D) Quantitative parameters of microtubule dynamics. Values are mean + SEM. (from Ye et al., 1998 [10])

Objectives:

1. To design novel derivative of Noscapine based on quantitative structure activity relationship of known Noscapine derivatives. To achieve this objective we will first determine the bioactive conformation of Noscapine derivatives using quantum mechanics optimization in reference to experimentally determined Noscapine structure. The IC_{50} value of these derivatives with a cancer cell line will be determined and will be used for developing QSAR model. Based on the QSAR model new derivatives of Noscapine will be designed and will be chemically synthesized and experimentally evaluated.

2. To computationally analyze the isotype specific β-tubulin interaction of tubulin heterodimer with Noscapinoids. To achieve this, a set of already known Noscapine derivatives will be used to study the molecular interactions. Towards this end the molecular structures of tubulin dimers composed of α- and different β-tubulin isotypes will be modelled based on the crystal structure of tubulin. The binding affinity of Noscapinoids with each type of tubulin will be evaluated using molecular docking. In particular the specific interaction of $\alpha\beta_{III}$- tubulin isotype (overexpression of $\alpha\beta_{III}$ has been associated with resistance to a wide range of chemotherapeutic drugs for several human malignancies) with Noscapine, amino-Noscapine (the most potent derivative) and bromo Noscapine (the clinical derivative) will be investigated using robust molecular modelling calculations such as molecular mechanics generalized Born solvation area (MMGBSA) and molecular mechanics Poisson-Boltzman solvation area (MMPBSA).

3. To design novel derivatives of Noscapine using structure based computer aided molecular designing techniques followed by chemical synthesis and experimental evaluation. Towards this end, first a library of Noscapine derivatives will be developed by substituting various functional groups in the scaffold structure of Noscapine using combinatorial chemistry. These derivatives will be virtually screened based on their binding affinity with tubulin based on molecular docking and more robust LIE-SGB calculation. The potent derivatives with improved binding affinity onto tubulin will be selected, chemically synthesized and experimentally evaluated for cell cytotoxicity, tubulin binding activity and toxicity.

CHAPTER 1 - Rational design of novel Noscapinoids using ligand based (QSAR) approach, their theoretical evaluation, chemical synthesis and biological evaluation.

Availability of structure activity data of batteries of Noscapinoids led to development of quantitative structure activity relationship (QSAR) model for the designing of novel Noscapine derivative. The data set used for QSAR model development in this study consists of previously reported 32 Noscapine derivatives (Table 1). All these compounds were obtained in synthetic form from Department of Cell Biology, Emory University School of Medicine, Georgia, USA and the compound 1 was purchased from Sigma-Aldrich. The antiproliferative activity of these compounds was determined using CEM (human lymphoblastoid) cancer cell line by MTS assay. The negative logarithm of IC_{50} value in molar concentrations ($pIC_{50} = - (\log_{10} IC_{50})$) of these compounds was used as response for QSAR model building.

Table 1. Chemical structures of Noscapine and its congeners used in the present study along with their observed inhibitory activity of CEM (human lymphoblastoid) cancer cell line proliferation.

Sl No.	Compound structure	IC_{50} (M)	Sl No.	Compound Structure	IC_{50} (M)
1	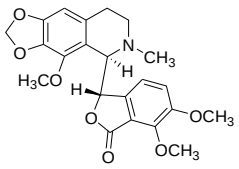	16.59×10^{-6}	2	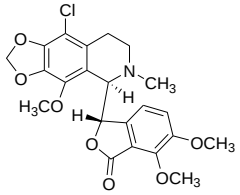	1.2×10^{-6}
3	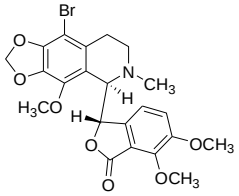	1.9×10^{-6}	4	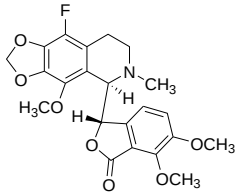	2.3×10^{-6}
5	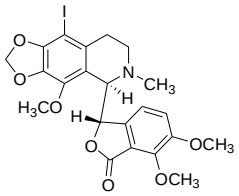	38.9×10^{-6}	6	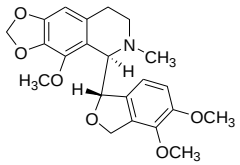	28.3×10^{-6}
7	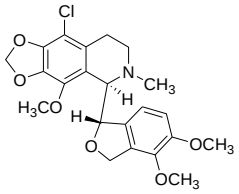	45.2×10^{-6}	8	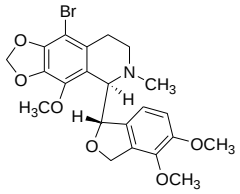	2.8×10^{-6}
9	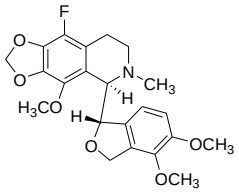	15.5×10^{-6}	10	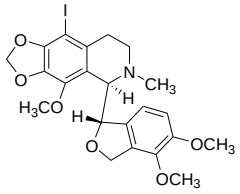	30.5×10^{-6}

11	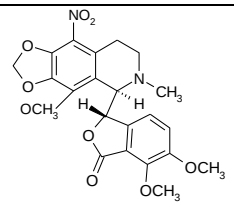	10.0×10^{-6}	12	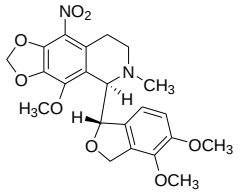	10.0×10^{-6}
13	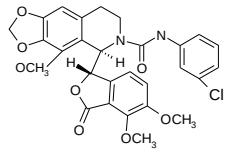	48.0×10^{-6}	14	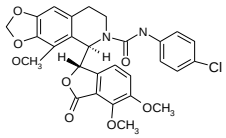	45.2×10^{-6}
15	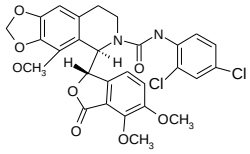	44.2×10^{-6}	16	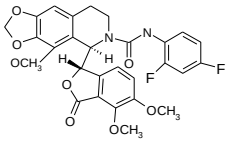	40.6×10^{-6}
17	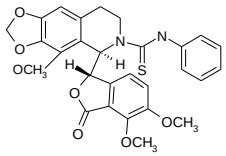	41.9×10^{-6}	18	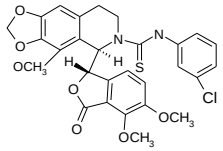	45.1×10^{-6}
19	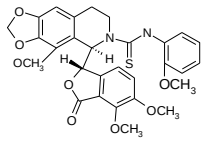	46.5×10^{-6}	20	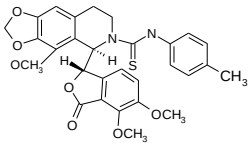	44.4×10^{-6}
21	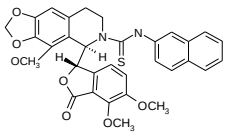	44.1×10^{-6}	22	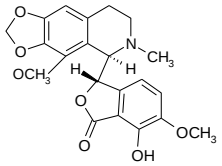	51.8×10^{-6}
23	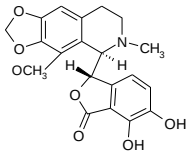	39.5×10^{-6}	24	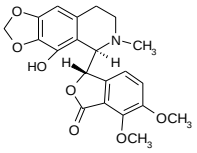	42.6×10^{-6}
25	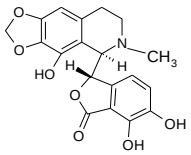	41.0×10^{-6}	26	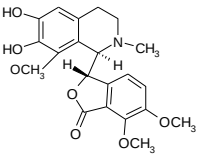	42.3×10^{-6}
27	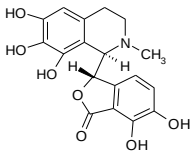	35.5×10^{-6}	28	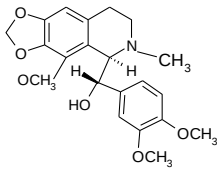	53.6×10^{-6}
29	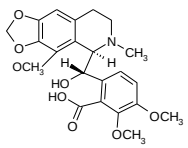	56.0×10^{-6}	30	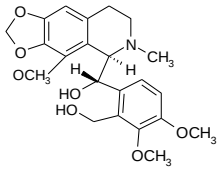	52.8×10^{-6}
31	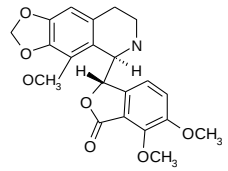	37.4×10^{-6}	32	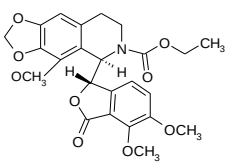	43.3×10^{-6}

The structure of Noscapine has two ring systems (isoquinoline and isobenzofuranone) joined by a rotatable single C-C bond between two chiral centers of the molecule. Noscapine might thus experience a diverse range of conformer states in solution. The stable state of the Noscapine was determined by X-ray crystallography as well as by two-dimensional NMR spectroscopy specially NOESY (Nuclear Overhauser and Exchange Spectroscopy). The dynamic range of structures obtained by 2D NMR in solution was integrated using NAMFIS (NMR Analysis of Molecular Flexibility In Solution). Both the crystal structure and NAMFIS have determined a completely extended outstretched "open-palm (two ring planes at approximately 108^{o})" conformation to Noscapine. Out of many conformations generated, Noscapine spends majority of its time (86%) in "open-palm" conformations. Similar conformation of all the derivatives were generated based on *Ab initio* quantum mechanics calculations using B3LYP and basis set 3-21G* level. (Figure 2)

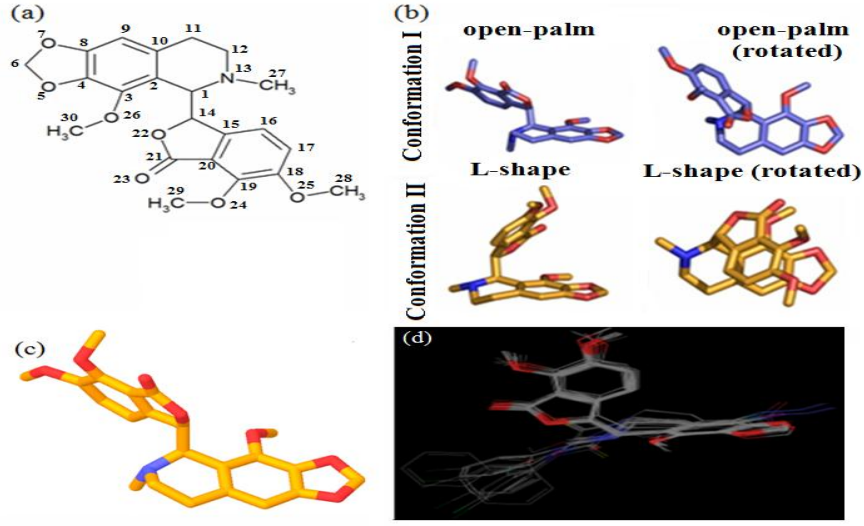

Figure 2.(a) Structure of noscapine with atomic numbers used in this study. (b) Two probable Noscapine conformations in solution derived from the NOESY spectra followed by NAMFIS analysis: conformation I is an open-palm conformation (exists 86% of time in solution) and conformation II is a closed-palm conformation (a tilted L-shaped conformation that exists 13% of time in solution). The rotated versions of these two conformations are shown on the right. (c) The geometrically optimized Jaguar generated conformation of noscapine also comfortably revealed open-palm conformation. (d) Superposition of geometrically optimized conformations of noscapinoids (32 molecules) revealed similar scaffold.

Different classes of molecular descriptors were calculated from the structures obtained above using molecular operating environment (MOE, version 2009-2010) software. A systematic search in the order of missing value test, zero test, correlation coefficient and genetic function approximation (GFA) was performed to determine significant descriptors from each class of descriptor for QSAR model building. Genetic function approximation algorithm of variable selection was used to generate the QSAR model. The predictive capability of the developed QSAR model was validated based on several statistical tests such as leave-one-out, leave-10%-out, leave-20%-out cross validation and Y-randomization test.

Results and discussion

The anti-tumor activities (IC_{50}) of 32 Noscapinoids determined using CEM cell line have a reasonably wide spectrum of anti-tumor activities (1.2 μM to 56.0 μM) (Table 1). To develop the QSAR model, 22 structures were used as a training set, while the remaining 10 structures as a test set. The geometrically optimized structures of the molecules obtained in reference to the experimental structure of Noscapine were used to calculate a set of 422 molecular descriptors. It includes a set of shape and topological descriptors, described by means of the surface area, volume, topological indices and dihedral angle between the isoquinoline and isobenzofuranone rings. The electronic descriptors such as E_{HOMO}, E_{LUMO}, local charges and dipole moments were derived from AM1 calculations. Indices of electronegativity ($\chi = -0.5(E_{HOMO} - E_{LUMO})$), hardness ($\eta = 0.5(E_{HOMO} - E_{LUMO})$), softness ($S = 1/\eta$) and electrophilicity ($\omega = \chi^2/2\eta$) were calculated from HOMO and LUMO energies [20]. Constitutional molecular descriptors were used to define the effect of different fragments of the molecules. From each class of molecular descriptors, significant descriptors were filtered out systematically as mentioned in materials and method section, pertaining to QSAR model development. Multiple linear regression (MLR) analyses were employed for QSAR model development (Table 2). Finally the QSAR model which was developed by combinig the descriptors from (Eqation 1-5, Table 2) which had high correlation with biological activity was selected.

$$pIC_{50} = 4.746\ (0.034) - 0.586\ (0.075) * \text{softness} + 0.664\ (0.253) * \text{vdw\_area} - 0.317\ (0.288) * \text{KierA3} + 0.241\ (0.071) * \text{SMB2} + 0.101\ (0.108) * \text{directional\_hyd\_sa} - 0.167\ (0.06) * \text{directional\_pol\_sa}$$

(N = 22, LOF = 0.123, $R^2 = 0.942$, $R^2_{adj} = 0.914$, $S = 0.159$, PRESS = 1.199, F-test = 34.42, P = 0.0001, $R^2_{LOO} = 0.815$, $RM^2 = 0.900$, $R^2_{test} = 0.817$)

where n is the number of compounds in the training set, R^2 is the squared correlation coefficient, S is the estimated standard deviation about the regression line, R^2_{adj} is the square of the adjusted correlation coefficient for degrees of freedom, F-test is the measure of variance that compares 2 models differing by one or more variables to determine if the complexity of the model correlates positively with its reliability (the model is supposed to be good if the F test is above a threshold value), and R^2_{LOO} is the square of the correlation coefficient of the cross-validation using the leave-one-out (LOO) cross-validation technique.

The QSAR model developed in this study is statistically best fitted ($R^2 = 0.942$, $R^2_{LOO} = 0.815$, F-test = 34.42) and consequently used for the prediction of anti-tumor activities (pIC_{50}) of training and test sets of molecules as reported in Tables 3 and 4. The quality of the prediction models for the training compounds is shown in Figure 3. The robustness of the QSAR model ($R^2 = 0.942$) was analyzed by values of the internal cross-validated regression coefficient ($R^2_{LOO} = 0.815$) for the training set. Satisfied with the robustness of the QSAR model developed using the training

set we next applied the QSAR model to an external data set of Noscapine analogues comprising the test set Table 4. The quality of the prediction models for the test compounds is shown in Figure 3.

Table 2. The results of multiple linear regression (MLR) analysis with different type of descriptors.

Sl. No.	MLR equations	Type of descriptors
1	pIC_{50} = 4.737(0.077)*VDistEq – 2.386(0.6631)*weinerPath + 1.53(0.428)* BCUT_SLOGP_1 + 0.169(0.101)*GCUT_SLOGP_1 (N = 22, LOF = 0.203, R^2 = 0.590, R^2_{adj} = 0.545, S = 0.373, PRESS = 4.264, F-test = 6.76, P = 0.001, R^2_{cv} = 0.418, RM^2 = 0.352, R^2_{test} = 0.529)	Topology
2	pIC_{50} = 4.793(0.076) + 3.897(1.118)*chi0v – 3.31(1.361)*chi1v + 0.967(2.395)*chi0 – 0.408(2.447)*Kier1 – 1.29(0.471)KierA3 (N = 22, LOF = 0.203, R^2 = 0.641, R^2_{adj} = 0.547, S = 0.373, PRESS = 4.261, F-test = 6.79, P = 0.001, R^2_{cv} = 0.421, RM^2 = 0.356, R^2_{test} = 0.537)	Shape
3	pIC_{50} = 4.761(0.073) – 1.62(0.456)*logS + 7.391(2.013)*MR – 9.349(1.779)*SMR - 0.124(0.113)*TPSA + 1.025(0.570)*vdw_area – 0.797(0.392)*log p(o/w) (N = 22, LOF = 0.202, R^2 = 0.688, R^2_{adj} = 0.584, S = 0.357, PRESS = 5.845, F-test = 6.62, P = 0.001, R^2_{cv} = 0.463, RM^2 = 0.434, R^2_{test} = 0.604)	Physical
4	pIC_{50} = 4.696(0.067) + 0.188(0.082)*SMB2 – 2.431(0.578)*SMB4 + 2.152(0.511)*SMB5 + 0.243(0.154)*directional_hyd_sa + 0.115(0.147)* directional_pol_sa (N = 22, LOF = 0.140, R^2 = 0.737, R^2_{adj} = 0.663, S = 0.322, PRESS = 3.302, F-test = 10.43, P = 0.0001, R^2_{cv} = 0.552, RM^2 = 0.572, R^2_{test} = 0.617)	Sterimol
5	pIC_{50} = 4.753(0.069) – 0.384(0.126)*Am1_dipole + 0.291(0.103)*E_rele + 0.106(0.098)*dipoleX + 22.766(6.369)*Electronegativity – 13.987(3.924)* Softness + 10.04(2.708)*Electrophilicity (N = 22, LOF = 0.140, R^2 = 0.749, R^2_{adj} = 0.665, S = 0.321, PRESS = 4.056, F-test = 8.94, P = 0.0001, R^2_{cv} = 0.449, RM^2 = 0.554, R^2_{test} = 0.679)	Quantum
6	pIC_{50} = 4.746(0.034) – 0.586(0.075)* softness + 0.664(0.253)*vdw_area - 0.317(0.288)*KierA3 + 0.241(0.071)*SMB2 + 0.101(0.108)* directional_hyd_sa – 0.167(0.06)* directional_pol_sa (N = 22, LOF = 0.123, R^2 = 0.942, R^2_{adj} = 0.914, S = 0.159, PRESS = 1.199, F-test = 34.42, P = 0.0001, R^2_{cv} = 0.815, RM^2 = 0.900, R^2_{test} = 0. 817)	All descriptor

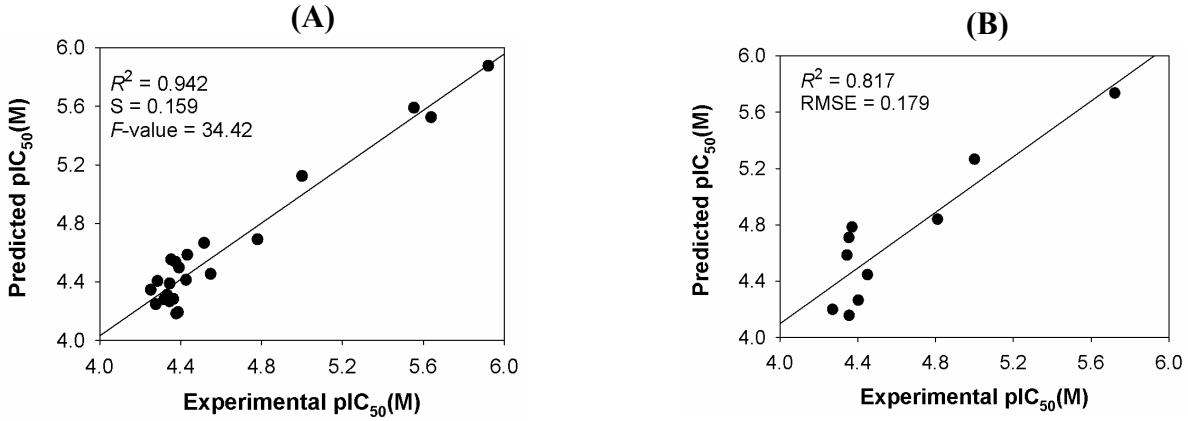

Figure 3.Relationship between predicted and experimental biological activities of(A) training set compounds as per QSAR equation (6). (B) test set compounds as per QSAR equation (6). Biological activities are pIC_{50}= -log (IC_{50}) in molar concentrations.

Table 3. Predicted anti-tumor activity of the training set compounds in Table 1 according to the QSAR models (using equations 2-6, Table 2).

Compound number	Experimental pIC_{50} (M)	Predicted pIC_{50} (M)				
		pIC_{50}^{2}	pIC_{50}^{3}	pIC_{50}^{4}	pIC_{50}^{5}	pIC_{50}^{6}
1	4.780	5.137	4.897	4.915	5.132	4.692
2	5.921	5.331	4.706	5.332	5.607	5.877
4	5.638	5.779	4.723	5.431	5.261	5.525
5	4.410	4.989	4.651	4.623	4.243	4.586
6	4.548	4.669	4.844	4.713	4.618	4.456
7	4.345	4.429	4.469	4.560	4.313	4.269
8	5.553	4.945	4.851	5.335	5.240	5.591
10	4.516	4.529	4.948	4.865	4.714	4.667
11	5.000	5.079	4.785	4.891	5.175	5.124
13	4.319	4.397	4.518	4.527	4.301	4.283
16	4.392	4.535	4.586	4.581	4.250	4.499
17	4.378	4.230	4.466	4.298	4.372	4.185
18	4.346	4.334	4.627	4.272	4.217	4.390
19	4.333	4.239	4.568	4.503	4.142	4.313
20	4.353	4.251	4.813	4.130	4.394	4.554
22	4.286	4.616	5.099	4.280	4.232	4.407
25	4.387	3.980	5.257	4.406	3.993	4.195
26	4.374	4.676	5.332	4.690	4.239	4.538
29	4.252	4.392	5.256	3.927	4.289	4.347
30	4.277	4.186	5.152	4.488	4.374	4.249
31	4.427	4.747	5.111	4.255	4.430	4.415
32	4.364	4.584	4.717	3.709	4.513	4.285

[2,3,4,5,6]Based on QSAR equation 2,3,4,5 and 6 developed in the study.

Table 4. Predicted anti-tumor activity of the test set compounds in Table 1 according to the QSAR models (using equations 2-6, Table 2).

Compound number	Experimental pIC_{50} (M)	Predicted pIC_{50} (M)				
		pIC_{50}^{2}	pIC_{50}^{3}	pIC_{50}^{4}	pIC_{50}^{5}	pIC_{50}^{6}
3	5.721	5.100	5.153	5.103	5.736	5.736
9	4.810	4.905	5.192	5.048	4.816	4.841
12	5.000	4.744	5.078	5.034	5.016	5.267
14	4.345	4.624	4.242	4.635	4.769	4.586
15	4.355	4.527	4.620	4.512	4.449	4.711
21	4.356	4.633	4.527	4.487	4.224	4.158
23	4.403	4.554	4.171	4.414	4.541	4.266
24	4.371	4.827	4.571	4.845	4.229	4.786
27	4.450	4.565	4.067	4.250	3.657	4.447
28	4.271	4.695	4.303	4.464	4.240	4.201

[2,3,4,5,6]Based on QSAR equation 2,3,4,5 and 6 developed in the study.

The estimated correlation coefficient between experimental and predicted pIC_{50} values with intercept (R^2) and without intercept (R^2_0) are 0.942 and 0.940, respectively. [20,21]. Values of R^2_{test}= 0. 817 and rm^2 = 0.90 were in the acceptable range thereby indicating the good external predictability of the QSAR model [20,21]. The appearance of the electronic descriptors such as electronegativity and electrophilicity in equation 5 as well as softness in equation 6 (calculated from

HOMO and LUMO energies) demonstrates that these descriptors significantly influence the anti-tumor activity of Noscapinoids. They favour columbic interaction between ligands and receptor. Therefore, the developed QSAR models guided us to substitute a functional group such as "azido" ($N^-=N^+=N^-$), satisfying the above descriptors in the scaffold structure of Noscapine pertaining to better anti-tumor activity. To begin to test this, I have built two Noscapine derivatives using molecular builder: 9-azido Noscapine and reduced-9-azido Noscapine (Table 5.) and predicted their biological activities by using QSAR model. Both molecules deduced to have superior activity in comparison to the lead molecule, Noscapine. To experimentally test the predictability of the QSAR model both the molecules were chemically synthesized (Scheme 1). The biological activity of the synthesized derivatives was experimentally determined in CEM cells using MTS assay in the similar conditions as the above mentioned 32 compounds. The predicted (5.731 and 5.710 M) and experimental (5.585 M) pIC_{50} values are included in Table 5. The experimental results (with extremely small deviations of 0.146 M and 0.125 M) show that the QSAR model has a highly predictive power for the further design of better Noscapinoids as well as would perform as a good rapid screening tool to uncover new and more potent anti-tumor drugs based on Noscapine derivatizations.

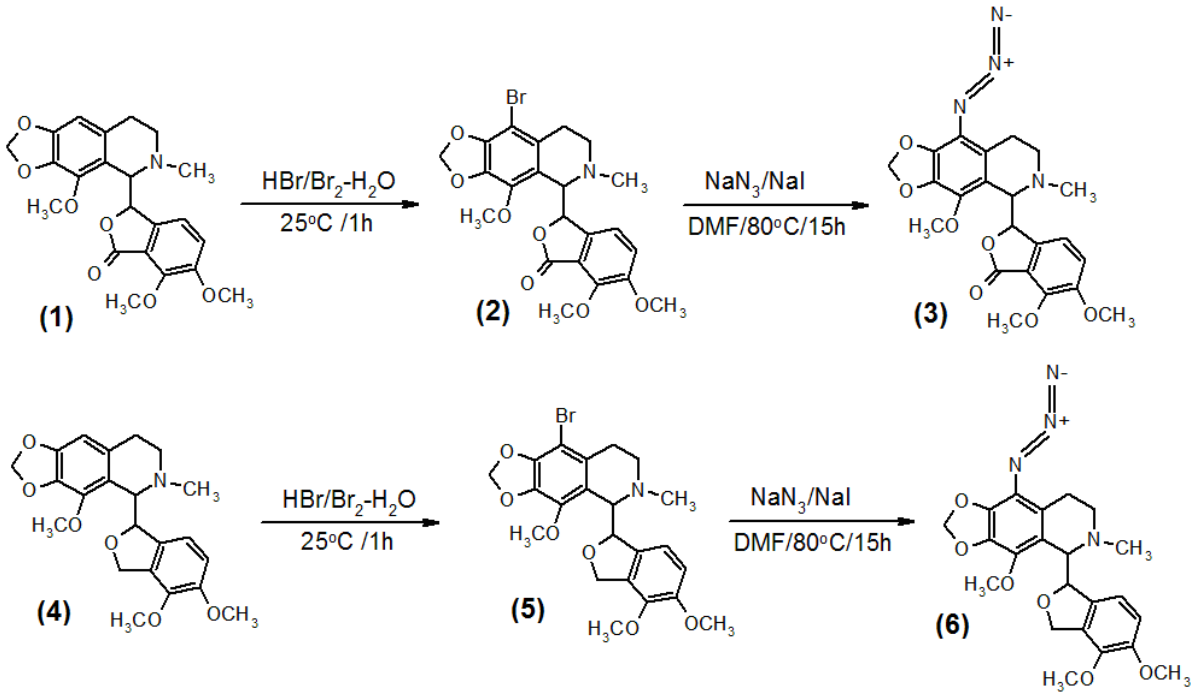

Scheme 1. Chemical synthesis of azido-Noscapine and reduced azido-Noscapine. 9-azido-noscapine yield, 89%; mp 177.2 to178.1 °C; IR: 1529, 1362 cm^{-1}; ^1H NMR ($CDCl_3$, 400 MHz): δ 7.05 (d, 1H, *J* = 7.0 Hz), 6.4 (d, 1H, *J* = 7.0 Hz), 6.01 (s, 2H), 5.85 (d, 1H, *J* = 4.4 Hz), 4.40 (d, 1H, *J* = 4.4 Hz), 4.15 (s, 3H), 3.88 (s, 3H), 3.84 (s, 3H), 2.75-2.62 (m, 2H), 2.60-2.56 (m, 2H), 2.51 (s, 3H); ^{13}C NMR ($CDCl_3$, 100 MHz): δ 169.2, 157.7, 152.6, 147.9, 142.2, 140.5, 135.0, 134.0, 123.5, 121.8, 119.7, 119.3, 114.1, 100.5, 87.4, 64.1, 56.7, 56.5, 56.2, 51.4, 39.2, 27.2; HRMS (ESI): *m/z* calculated for $C_{22}H_{23}N_4O_7$ (M+1), 455.4335;

experimentally determined, 455.4452 (M+1). Yield for compound reduced 9-azido-noscapine was 84%; mp 121 to 122 ^{0}C; IR: 1320, 1153 cm^{-1}; ^{1}H NMR ($CDCl_3$, 400 MHz): δ 6.74 (d, 1H, *J* = 8.0 Hz), 6.19 (d, 1H, *J* = 8.0 Hz), 6.06 (s, 2H), 5.48 (s, 2H), 4.88 (dd, 1H, *J* = 12 Hz), 4.77 (dd, 1H, *J* = 12 Hz), 4.75 (s, 1H), 3.82 (s, 6H), 3.79 (s, 3H), 3.38 to 3.15 (m, 2H), 2.95 (s, 3H), 2.78-2.80 (m, 2H); ^{13}C NMR ($CDCl_3$, 100 MHz), δ 153.5, 151.2, 149.3, 148.4, 135.9, 135.4, 132.5, 130.7, 120.5, 121.1, 114.0, 105.6, 100.8, 97.5, 68.9, 64.8, 56.5, 56.2, 55.6, 52.1, 40.9, 27.5; HRMS (ESI): *m/z* calculated for $C_{22}H_{23}N_4O_6$ (M+1), 441.4469; experimentally determined, 441.4453 (M+1).

Table 5. Predicted biological activity (pIC_{50}) obtained from the QSAR models (using equations 2-6) and experimental biological activity for the designed set of Noscapinoids.

Structure of the compound	**Experimental IC_{50} (M)**	**Experimental pIC_{50} (M)**	**Predicted pIC_{50} (M)**				
			pIC_{50}^2	**pIC_{50}^3**	**pIC_{50}^4**	**pIC_{50}^5**	**pIC_{50}^6**
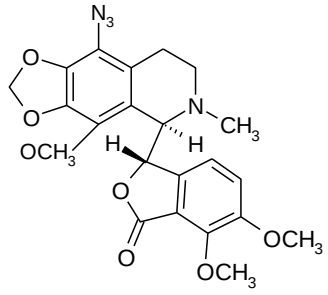 (9-azido-Noscapine)	2.6×10^{-6}	5.585	5.166	4.541	5.340	5.607	5.731
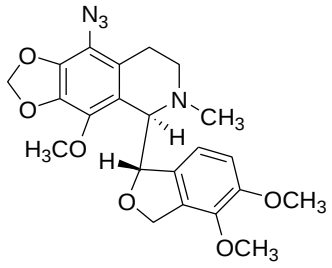 (Reduced 9-azido-Noscapine)	2.6×10^{-6}	5.585	5.629	4.624	5.626	5.709	5.710

Conclusion:

Firstly the bioactive conformation of Noscapine derivatives was obtained using quantum mechanics optimization in reference to experimentally determine Noscapine structure. Geometrical optimization was performed using semi-empirical quantum chemical calculations at 3-21G* level. Structures were in agreement with NMR Analysis of Molecular Flexibility in Solution--NAMFIS, and crystal structures. The IC_{50} value of these derivatives in human acute lymphoblastic leukemia cells (CEM) was determined and used for developing QSAR model. The IC_{50} values of these analogs vary from 1.2 to 56.0 μM. Genetic function approximation algorithm of variable selection was used to generate the QSAR model. The robustness of the QSAR model (R^2 = 0.942) was analyzed by values of the internal cross-validated regression coefficient (R^2_{LOO} = 0.815) for the training set and determination coefficient (R^2_{test} = 0.817) for the test set. Validation was achieved by rational design of further novel and potent anti-tumor Noscapinoid, 9-azido-Noscapine and reduced-

9-azido-Noscapine. These analogues were chemically synthesized based on their promising predicted activity and were further experimentally evaluated for cell cytotoxicity in human acute lymphoblastic leukemia cells (CEM). The experimentally determined value of pIC_{50} for both the compounds (5.585 M) turned out to be very close to predicted pIC_{50} (5.731 and 5.710 M).

CHAPTER 2 - Molecular insight of isotypes specific β-tubulin interaction of tubulin heterodimer with Noscapinoids.

Noscapine and its derivatives were demonstrated to bind stoichiometrically to tubulin, composed of α- and β-tubulin, which exist as various isotypes. The distribution of these isotypes is different among cells of different tissue of origin. Furthermore, their drug-binding properties are significantly different. Although the Noscapinoids were demonstrated to bind at the interphase of the two dimers, their interaction is more biased towards β-tubulin. Therefore, in this study, efforts have been made to investigate the mechanistic details of precise interaction and binding affinity of Noscapinoids with isotypes specific β-tubulin heterodimer. Understanding of molecular interactions of these agents onto tubulin isotypes would be important to improve the efficacy of Noscapinoids towards specific cancer type.

Material & Methods

The protein sequences of eight human β-tubulin isotypes (β_I to β_{VIII}): β_I (gi:18088719), β_{II} (gi:29788768), β_{III} (gi: 1297274), β_{IV} (gi: 135470), β_V (gi:14201536), β_{VI} (gi: 62903515), β_{VII} (gi:1857526) and β_{VIII} (gi:42558279) were aligned and compared to reveal any differences in the Noscapinoid binding site region [23,24]. Since the structures of αβ-tubulin isotype dimmers are not available, homology modeling was used to generate their structures. The co-crystallized structure of colchicine-tubulin complex (PDB ID: 1SA0, resolution 3.58 Å) was used as template for homology modeling of tubulin isotypes. However, the crystal structure was found to possess several errors: (a) the residues were not sequentially numbered in β chain (B chain), (b) some of the amino acids between 37 to 47 (α-tubulin) and 275 to 284 (β-tubulin) were found missing (Figure 4). In order to remove the errors the amino acids were renumbered and the gaps were filled by homology modeling based on PDB ID: 3DU7 (C-chain) and PDB ID: 3RYC (D-chain) respectively as templates for the gap regions using Prime (version 3.0, Schrödinger) (Figure 5). The modeled template structure was refined using energy minimization in Macromodel (version 9.9, Schrödinger) and by performing an all atom molecular dynamics (MD) simulation for a period of 10 ns using GROMACS 4.5.4 software and validated using structure validation programs like PROCHECK [25, 26], ERRAT [27] and VERIFY3D [28].

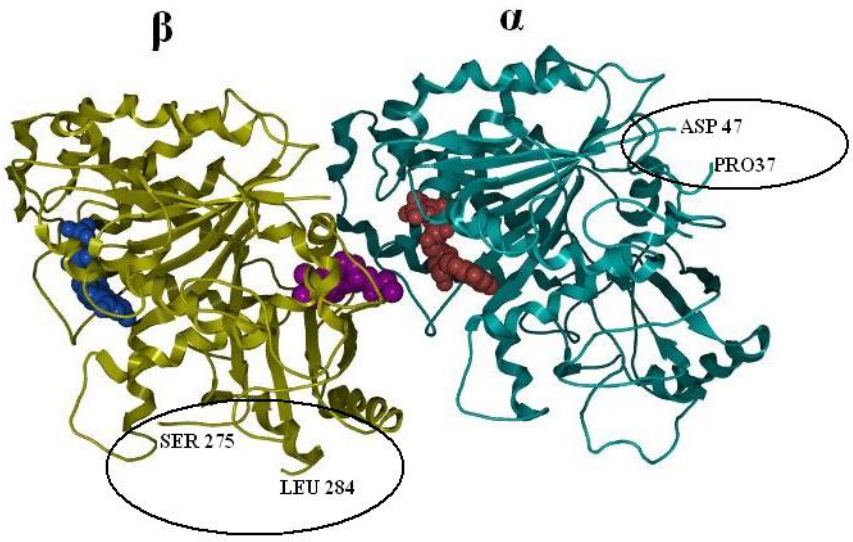

Figure 4. Representation of gaps (missing residues) in the crystal structure (1SA0) of tubulin dimer along with ligand colchicine (pink), GTP (Brown) and GDP (blue). The gaps (encircled) and the end residues of gaps ASP47 and PRO37 in α chain and SER275 and LEU384 in β chain are shown in the figure.

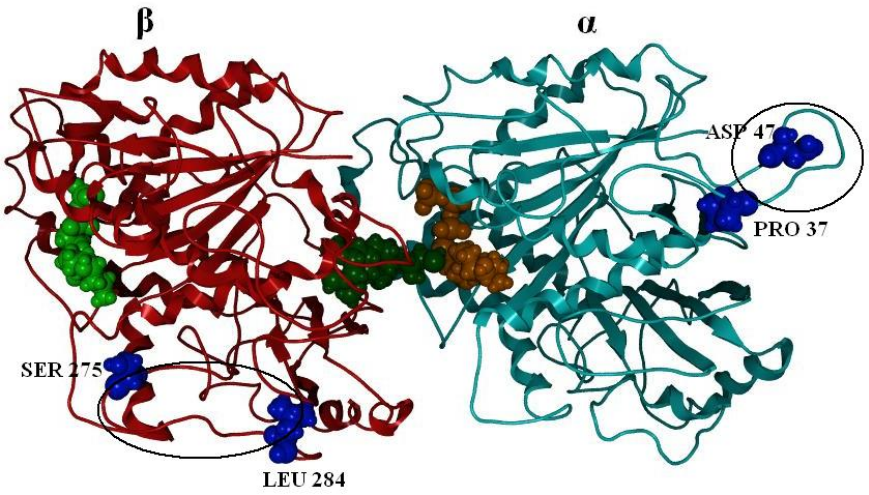

Figure 5. Modelled tubulin dimer along with ligand colchicine(dark green), GTP (Brown) and GDP (light green) having no gaps as evident from the figure. Gaps between the end residues of ASP 47 and PRO 37 in α chain and SER275 and LEU384 in β chain were filled as loops (encircled portion).

The structures of different tubulin isotypes were build based on the above prepared and refined structure of tubulin, using Prime (version 3.0, Schrödinger). Furthermore, the modelled structures of the tubulin isotypes were refined by performing an all atom MD simulation of 10 ns as described previously. Stable structures of isotypes were generated from the last 2000 frames of the MD trajectory. The quality of the modelled structures of tubulin isotypes was evaluated using PROCHECK, ERRAT and VERIFY3D. Different binding sites were predicted and analyzed for the modeled αβ-tubulin isotypes using SiteMap (version 2.4, Schrodinger). However, only the Noscapinoid binding site [24] (at the interface between α- and β-tubulin) for each protein structure was selected for comparative analysis and predicting binding affinity of Noscapinoids. For the

binding affinity calculations, molecular structures of Noscapine and its derivatives (Figure 6) that were previously demonstrated to be tubulin binding agents [17,29-33] were built, energy minimized and geometrically optimized using Jaguar (version 7.7, Schrödinger, LLC). Molecular docking using "Extra Precision" (XP) algorithm of Glide docking (version 5.7, Schrödinger) [34,35] was used to calculate the binding affinity of these Noscapinoids onto tubulin isotypes.

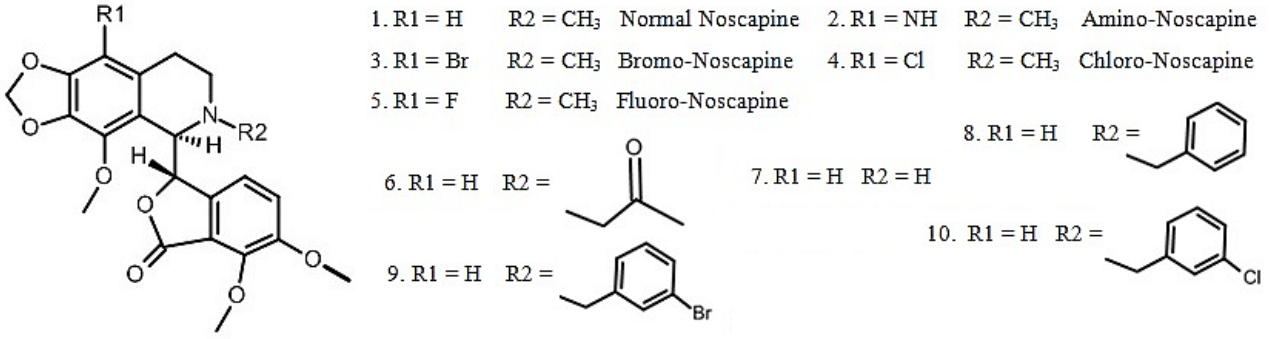

Figure 6 Chemical structure of Noscapine and its derivatives used in the study. These derivatives were previously demonstrated to be tubulin-binding agents.

Out of different αβ-tubulin isotypes, researchers have already realized that $\alpha\beta_{III}$ would be an excellent target for anti-tumor drugs as $\alpha\beta_{III}$ has been associated with resistance to a wide range of chemotherapeutic drugs for several human malignancies [36-41]. Also efforts are already being made to create a $\alpha\beta_{III}$-specific drug [42]. Reports also shown that Noscapinoids have shown promising results with drug resistant cancer cell lines. Motivated by the above facts, I have narrowed down my focus towards the specific interaction of $\alpha\beta_{III}$ –tubulin isotype with Noscapine, amino Noscapine (the most potent derivative) and bromo Noscapine (the clinical derivative). For binding affinity calculations, docking complexes of $\alpha\beta_{III}$ isotype with amino-Noscapine, bromo-Noscapine and Noscapine, were extracted and MD simulation for a period of 10 ns was performed in AMBER 11.0 [43] software suite. A total of 1000 snapshots generated from the last 2 ns of the MD trajectory for each molecular species were selected to calculate the binding free energy based on molecular mechanics generalized Born solvation area (MM-GBSA) and molecular mechanics Poisson Boltzmann solvation area (MM-PBSA) [44,45]. To achieve the detailed view of the interaction of Noscapinoids with $\alpha\beta_{III}$ isotype, the binding free-energy contribution of each residue was computed using MM-GBSA model.

Results and Discussions

Comparison of the sequences of eight human β-tubulin isotypes (β_I to β_{VIII}) revealed significant differences especially in the Noscapinoid binding site region [24] (Table 6) which could affect the binding preferences of these isotypes towards Noscapinoids.

Table 6: Mismatches in amino acids comprising the Noscapinoid binding site [24] among different β isotypes in comparison to the template (1SA0). There are six positions (such as 236, 239, 315, 316, 351 and 368) where there are no clear consensuses in residues over all the β-isotypes.

Isotype	**Amino acid position**															
	179(A)	235	236	237	239	246	248	252	253	314	315	316	350	351	366	368
1SA0	Thr	Gly	Val	Thr	Cys	Leu	Ala	Lys	Leu	Ala	Ala	Val	Lys	Thr	Thr	Ile
β_{I}	Thr	Gly	Val	Thr	Cys	Leu	Ala	Lys	Leu	Ala	Ala	Val	Lys	Thr	Thr	Ile
β_{II}	Thr	Gly	Val	Thr	Cys	Leu	Ala	Lys	Leu	Ala	Ala	**Ile**	Lys	Thr	Thr	Ile
β_{III}	Thr	Gly	Val	Thr	**Ser**	Leu	Ala	Lys	Leu	Ala	**Thr**	Val	Lys	**Val**	Thr	Ile
β_{IV}	Thr	Gly	Val	Thr	Cys	Leu	Ala	Lys	Leu	Ala	Ala	Val	Lys	Thr	Thr	Ile
β_{V}	Thr	Gly	Val	Thr	**Ser**	Leu	Ala	Lys	Leu	Ala	**Thr**	Val	Lys	**Val**	Thr	Ile
β_{VI}	Thr	Gly	**Ile**	Thr	**Ser**	Leu	Ala	Lys	Leu	Ala	**Cys**	**Ile**	Lys	**Val**	Thr	Ile
β_{VII}	Thr	Gly	Val	Thr	Cys	Leu	Ala	Lys	Leu	Ala	Ala	**Ile**	Lys	Thr	Thr	**Thr**
β_{VIII}	Thr	Gly	Val	Thr	Cys	Leu	Ala	Lys	Leu	Ala	Ala	**Ile**	Lys	Thr	Thr	Ile

The structures of various αβ-tubulin isotypes were modeled based on the crystal structure of tubulin. The structures although showed structural similarity with the template but pairwise comparative analysis of these αβ-tubulin isotypes revealed significant variations with RMSD values in the range of 0.963-1.511 Å (Figure 7) (Table 7). The comparative structural and physico-chemical property analysis, using Sitemap, of the Noscapinoids binding site [24] from different αβ-tubulin isotypes revealed significant differences in the binding site (Table 8). The analysis of binding site structure by comparison of the amino acids within 12 Å diameter of Noscapinoid binding also revealed significant differences with RMSD of 0.655-1.352 Å (Table 9). The differences in conformation, composition and overall environment of the binding site among αβ-tubulin isotypes indicated differential binding affinities of Noscapinoids towards different isotypes.

Table 7: All-vs-all structure comparison of the αβ-tubulin isotypes. The values are root mean square deviation (RMSD) calculated by superimposition of the structures.

Isotypes	**$\alpha\beta_{I}$**	**$\alpha\beta_{II}$**	**$\alpha\beta_{III}$**	**$\alpha\beta_{IV}$**	**$\alpha\beta_{V}$**	**$\alpha\beta_{VI}$**	**$\alpha\beta_{VII}$**	**$\alpha\beta_{VIII}$**
$\alpha\beta_{I}$	0							
$\alpha\beta_{II}$	0.963	0						
$\alpha\beta_{III}$	1.200	1.136	0					
$\alpha\beta_{IV}$	1.145	1.139	1.127	0				
$\alpha\beta_{V}$	1.261	1.318	1.055	1.177	0			
$\alpha\beta_{VI}$	1.481	1.461	1.244	1.257	1.130	0		
$\alpha\beta_{VII}$	1.511	1.423	1.139	1.337	1.359	1.339	0	
$\alpha\beta_{VIII}$	1.351	1.277	0.943	1.216	1.152	1.244	1.054	0

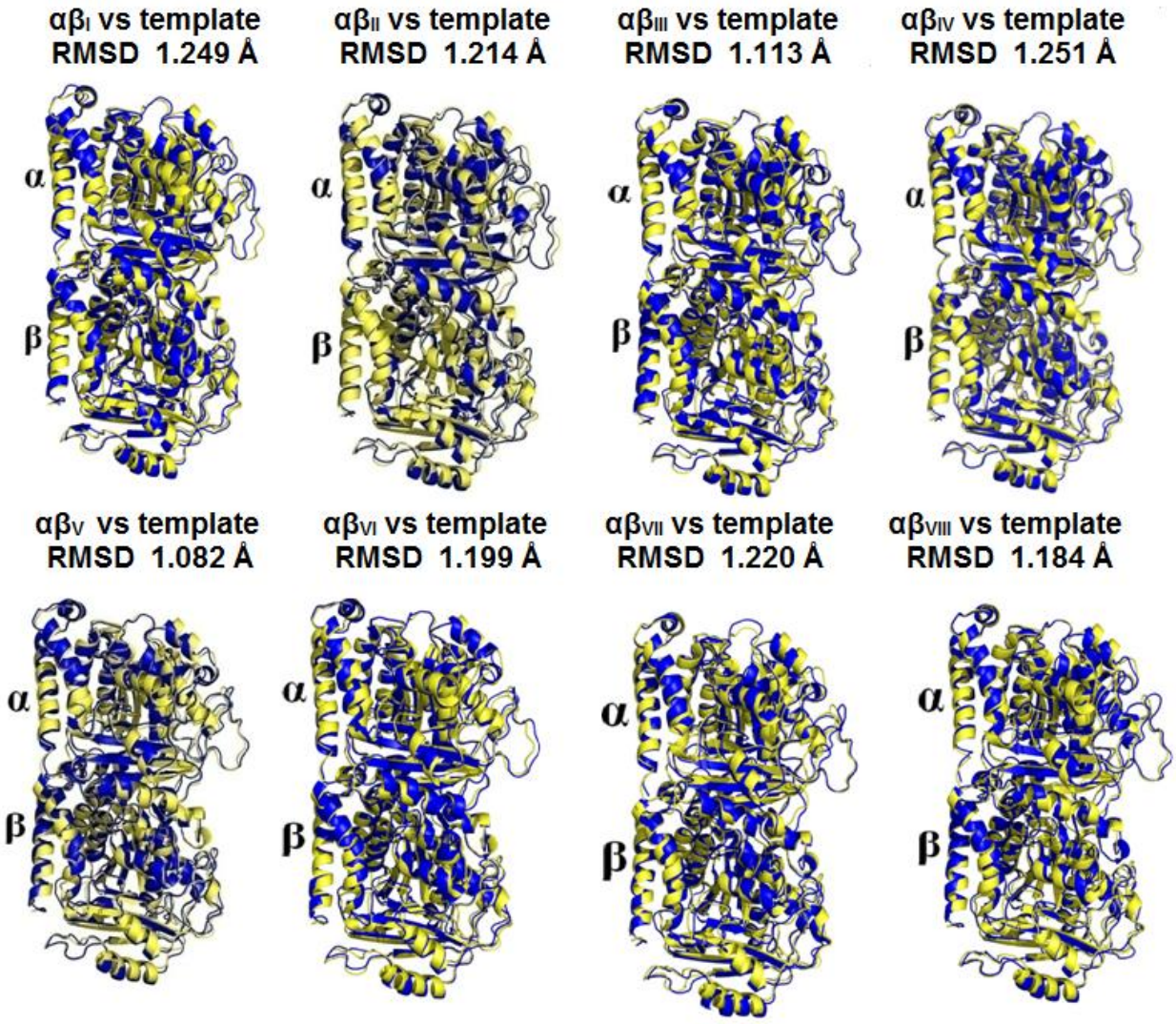

Figure 7. Superimposition of αβ-tubulin isotypes ($\alpha\beta_I$ to $\alpha\beta V_{III}$, blue) with the template structure (1SA0, yellow). The RMSD values ranges from 1.082-1.251 Å.

Table 8: Physico-chemical properties of the Noscapinoid bind site of different αβ-tubulin isotypes. The differences in binding site are due to the different composition of the binding site residues within and near the binding site region.

Isotype	SiteScore (a.u)	Volume(Å)^3	Exposure (a.u)	Enclosure (a.u)	Contact (a.u)	Phobic (kcal/mol)	Philic (kcal/mol)	Balance (a.u)	don/acc (a.u)
$\alpha\beta_I$	0.576	138.23	0.654	0.653	0.772	0.806	0.86	0.936	0.898
$\alpha\beta_{II}$	0.820	160.87	0.5	0.663	0.867	1.053	0.61	1.737	0.710
$\alpha\beta_{III}$	0.660	109.76	0.705	0.620	0.656	0.469	0.53	0.883	1.418
$\alpha\beta_{IV}$	0.743	171.16	0.550	0.593	0.741	0.886	0.62	1.439	1.438
$\alpha\beta_V$	0.634	122.45	0.629	0.629	0.805	0.611	0.80	0.762	1.261
$\alpha\beta_{VI}$	0.698	134.80	0.680	0.596	0.769	1.166	0.54	2.145	0.943
$\alpha\beta_{VII}$	0.735	126.91	0.426	0.663	0.905	1.343	0.58	2.299	1.641
$\alpha\beta_{VIII}$	0.588	91.581	0.561	0.653	0.814	0.749	0.80	0.938	2.279

Table 9: All-vs-all comparison of the amino acids within 12 Å diameter of Noscapinoid binding site of the different αβ-tubulin isotypes. The variation in the structure is measured by RMSD score after superimposition.

Isotypes	**$\alpha\beta_{I}$**	**$\alpha\beta_{II}$**	**$\alpha\beta_{III}$**	**$\alpha\beta_{IV}$**	**$\alpha\beta_{V}$**	**$\alpha\beta_{VI}$**	**$\alpha\beta_{VII}$**	**$\alpha\beta_{VIII}$**
$\alpha\beta_{I}$	0							
$\alpha\beta_{II}$	0.881	0						
$\alpha\beta_{III}$	1.110	0.750	0					
$\alpha\beta_{IV}$	0.865	0.662	0.761	0				
$\alpha\beta_{V}$	1.251	0.861	0.620	1.046	0			
$\alpha\beta_{VI}$	1.340	1.049	1.148	1.205	1.345	0		
$\alpha\beta_{VII}$	0.945	0.868	0.926	0.947	1.032	1.352	0	
$\alpha\beta_{VIII}$	1.066	0.655	0.701	0.746	0.808	1.144	0.969	0

The binding affinity of Noscapinoids onto the Noscapinoid binding site among different αβ-tubulin isotypes was determined using molecular docking. All the Noscapinoids showed significant differences in binding score (Table 10) with respect to different αβ-tubulin isotypes. The simplest reason could be the difference in binding mode of Noscapinoids among different isotypes mainly because of the differences in binding site amino acids. Analysis of the electrostatic and van der Walls energy contribution of residues within 12 Å diameter of Noscapinoid binding site [24], revealed differences in the contribution pattern. The differential binding affinity and mode of interaction of Noscapinoids suggests different specificity of Noscapinoids across different αβ-tubulin isotypes.

Table 10: Docking results (Glide XP) of Noscapinoids with different αβ-tubulin isotypes. All the Noscapinoids bind well with different isotypes. However, each Noscapinoid showed different docking score with respect to different αβ-tubulin isotypes. Overall amino-Noscapine and the clinical derivative, bromo-Noscapine showed better docking score against $\alpha\beta_{III}$-tubulin isotype in comparison to other isotypes.

	Docking score(kcal/mol)									
ISOTYPE	1	2	3	4	5	6	7	8	9	10
$\alpha\beta_{I}$	-5.278	-6.432	-5.601	-5.803	-5.213	-5.448	-5.039	-5.765	-6.328	-6.261
$\alpha\beta_{II}$	-6.671	-7.179	-6.897	-6.530	-6.851	-5.802	-6.327	-7.152	-7.147	-7.090
$\alpha\beta_{III}$	-5.278	-7.416	-7.242	-5.764	-5.496	-6.202	-5.151	-7.149	-7.126	-7.136
$\alpha\beta_{IV}$	-5.963	-7.317	-6.415	-6.617	-5.598	-3.084	-5.984	-6.312	-7.188	-6.364
$\alpha\beta_{V}$	-6.286	-5.453	-5.477	-6.270	-5.368	-6.280	-4.290	-6.086	-5.723	-6.792
$\alpha\beta_{VI}$	-5.903	-5.831	-5.763	-5.832	-6.560	-5.330	-7.148	-7.182	-7.010	-6.874
$\alpha\beta_{VII}$	-6.041	-6.351	-5.233	-6.506	-7.102	-4.547	-5.853	-7.136	-3.518	-6.371
$\alpha\beta_{VIII}$	-7.111	-6.804	-6.539	-6.068	-5.416	-5.706	-6.779	-7.236	-7.108	-7.205

Further I have narrowed down my focus on $\alpha\beta_{III}$-tubulin isotype to specifically study its interaction with Noscapine and two of its derivatives amino-Noscapine and bromo-Noscapine. In fact both amino-Noscapine and bromo-Noscapine showed highest docking score of -7.416 and -7.242 kcal/mol against this isotype in comparison to others. Inspired by the docking result I have

determined their preferred binding mode and binding affinity with $\alpha\beta_{III}$ by performing 10 ns of MD simulation (Figure 8). Analysis of the MD trajectories suggested that the binding site residues seem to be more rigid as a result of binding. The MD simulated complexes were subjected to binding affinity calculations based on MM-PBSA and MM-GBSA of Noscapine, amino-Noscapine and bromo-Noscapine with $\alpha\beta_{III}$ were summarized in Table 11.

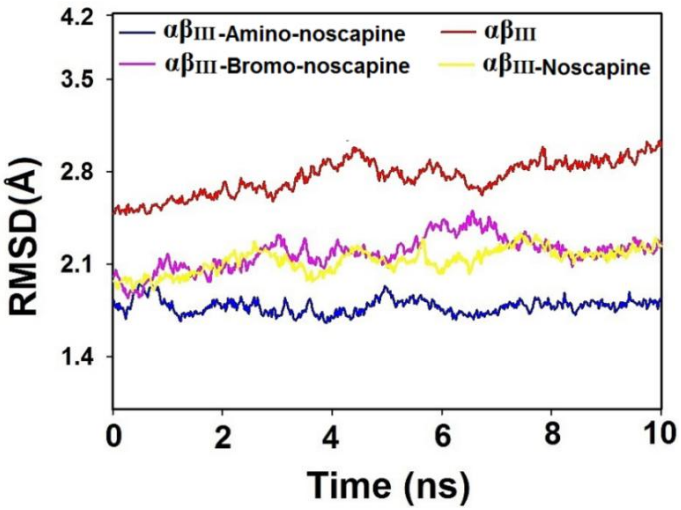

Figure 8. The root-mean square deviations (RMSD) of Cα carbon atoms of tubulin during 10 ns of MD simulation, starting from the docking complexes of $\alpha\beta_{III}$ with amino-Noscapine, bromo-Noscapine and Noscapine. The relative fluctuation in the RMSD of the Cα atoms is very small after ~8 ns of the simulation, demonstrating the convergence of the simulation. A 10 ns MD simulation was carried out with a time step of 2 fs, a total of 5000 frames were generated and the last 1000 frames from each molecular species were used to generate the average structure.

Table 11: Binding free energy and its components (kcal/mol) for the receptor, $\alpha\beta_{III}$ heterodimer and Noscapine derivatives.

Energy components (kcal/mol)	**Noscapine**	**Bromo-Noscapine**	**Amino-Noscapine**
ΔE_{ele}	-325.4	-337.2	-348.8
ΔE_{vdw}	-56.22	-60.86	-57.42
ΔE_{gas}	-381.6	-398.0	-406.2
$\Delta G_{sol\text{-}np}$	-6.530	-6.120	-6.370
ΔG_{PB}	357.9	370.0	375.6
$\Delta G_{solv,PB}$	353.6	365.9	371.5
$\Delta G_{ele,PB}$	32.49	32.89	26.76
$\Delta G_{bind,\ PB}$	**-28.02**	**-32.05**	**-34.70**
ΔG_{GB}	349.3	366.0	366.4
$\Delta G_{solv,GB}$	342.7	359.9	360.0
$\Delta G_{ele,\ GB}$	23.87	28.88	17.52
$\Delta G_{bind,\ GB}$	**-38.86**	**-38.09**	**-46.23**

All the three ligands showed better binding affinity with $\alpha\beta_{III}$ in the pattern of amino-Noscapine (-34.70 and -46.23 kcal/mol), bromo-Noscapine (-32.05 and -38.09 kcal/mol) and

Noscapine (-28.02 and -38.86 kcal/mol) based on both MM-PBSA and MM-GBSA calculations. All the three ligands (Noscapine, bromo-Noscapine and amino-Noscapine) were also well accommodated into the binding site of $\alpha\beta_{III}$-tubulin isotype, at the interface between α- and β-tubulin, however, their binding interactions with the amino acids inside the binding cavity were distinct. Residues that have the greatest impact, in terms of total energy (δG_{bind}) contribution (per residue contribution ≤ -1 kcal/mol) were identified. Although the binding site residues of $\alpha\beta_{III}$-tubulin isotype contributed differently towards binding to the three different ligands. However, some of the amino acids, Ser 239, Leu253, Ile 368, consistently contributed to the binding energy for all the three ligands, indicating their importance in their interaction with the ligands targeted towards $\alpha\beta_{III}$-tubulin isotype (Figure 9). The information gained in this study could pave a way for more efficient design of novel Noscapinoid, which could be specifically targeted towards cancer cells.

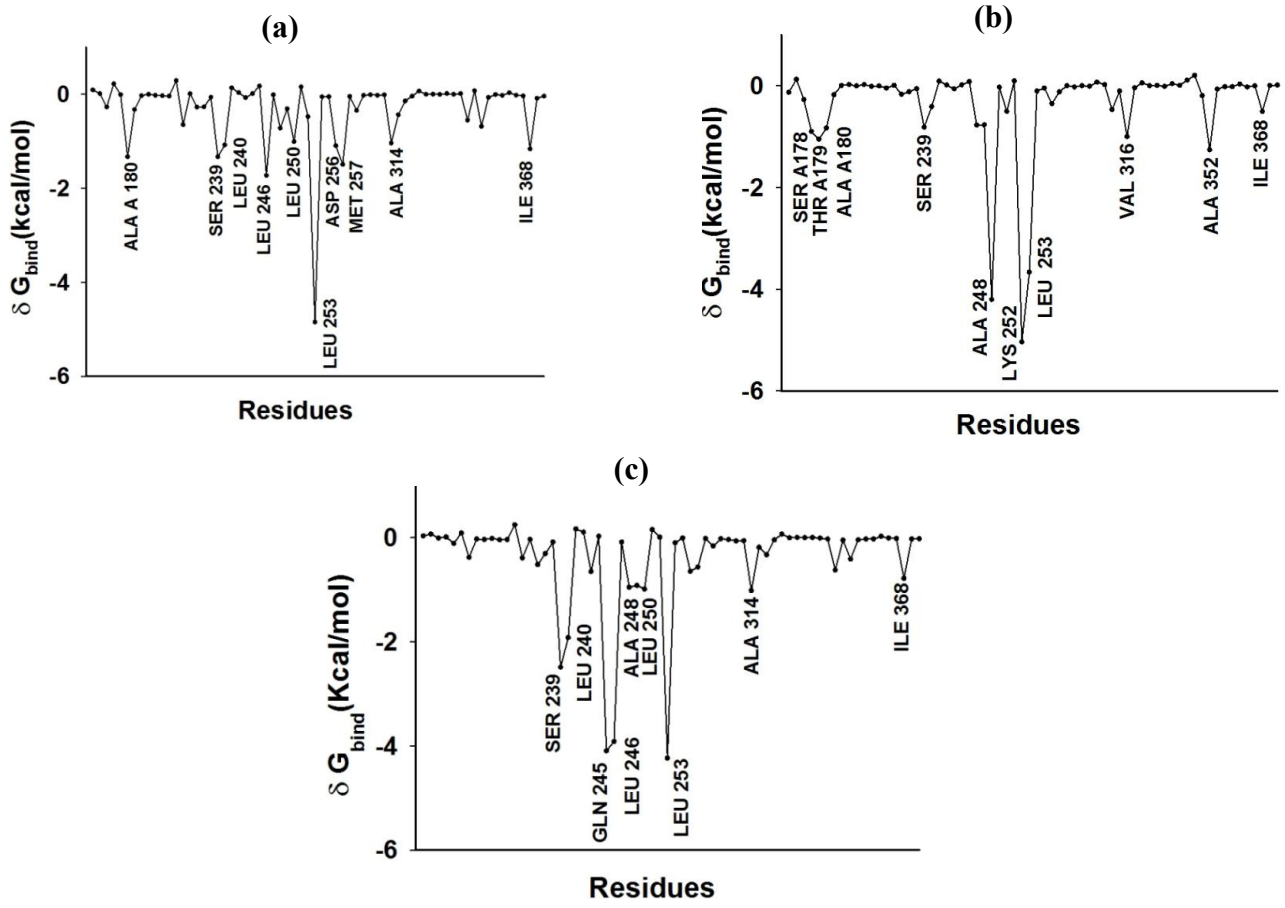

Figure 9. Per residue binding free energy (δG_{bind}) contribution of $\alpha\beta_{III}$ for the binding of (a) Noscapine, (b) bromo Noscapine and (c) amino Noscapine. The amino acids within 12 Å of the binding site were only considered.

Conclusion: In this study, the binding affinity of a panel of Noscapinoids with each type of tubulin is investigated computationally. We found that the binding score of a specific Noscapinoid with each type of tubulin isotype is different. Specifically, amino Noscapine has the highest binding

score of -6.432, -7.179, -7.416 and -7.417 kcal/mol with $\alpha\beta_I$, $\alpha\beta_{II}$, $\alpha\beta_{III}$ and $\alpha\beta_{IV}$ isotypes, respectively. Similarly **10** showed higher binding affinity of -6.792 kcal/mol with $\alpha\beta_{V,}$ whereas **8** has highest binding affinity of-7.182, -7.136 and -7.236 kcal/mol, respectively with $\alpha\beta_{VI}$, $\alpha\beta_{VII}$ and $\alpha\beta_{VIII}$ isotypes. More importantly, both amino Noscapine and the clinical derivative, bromo Noscapine have the highest binding affinity of -46.23 and -38.09 kcal/mol against $\alpha\beta_{III}$ (overexpression of $\alpha\beta_{III}$ has been associated with resistance to a wide range of chemotherapeutic drugs for several human malignancies) as measured using MM-PBSA. Knowledge of the isotype specificity of Noscapinoid may allow for development of novel therapeutic agents based on this drug.

CHAPTER 3 – Structure based design of novel Noscapinoids, theoretical evaluation, chemical synthesis and experimental evaluation.

Materials and methods

A library of Noscapine derivatives was developed by substituting various functional groups in the scaffold structure of natural α-Noscapine using combichem module of Schrodinger. Further a set of already reported Noscapine derivatives [18,19,30-33] (Figure 10) with known tubulin binding affinity (K_d value) was used as training set to develop the predictive model for the screening of potent derivatives. Molecular structures of all these derivatives along with the newly designed derivatives were geometrically optimized using Jaguar and docked onto the Noscapinoids binding site using Glide XP (Schrodinger). Further the docked complexes of Noscapinoids were energy minimized using hybrid Monte Carlo and molecular dynamics simulation to calculate various energy parameters (U_{vdw}, U_{elec} and U_{cav}) applying surface generalized Born (SGB) continuum solvation model. These energies parameters of the training set molecules were used to develop linear interaction energy (LIE) predictive model [46] for the prediction of binding affinity of newly designed derivatives as follows.

$$\Delta G_{bind} = \alpha\left(\langle U^b_{vdw}\rangle - \langle U^f_{vdw}\rangle\right) + \beta\left(\langle U^b_{elec}\rangle - \langle U^f_{elec}\rangle\right) + \gamma\left(\langle U^b_{cav}\rangle - \langle U^f_{cav}\rangle\right) \qquad \textbf{(1)}$$

Here $\langle\ \rangle$ represent the ensemble average, *b* represents the bound form of the ligand, *f* represents the free form of the ligand, and α, β, and γ are the coefficients. U_{vdw}, U_{elec}, and U_{cav} are the van der Waals, electrostatic, and cavity energy terms in the SGB continuum solvent model. Based on the predictive binding free energy, a set of six newly designed derivatives **5a-5f** (Figure 11), which have better binding free energy compared to the lead molecule were finally selected. To further refine the binding free energy score of these derivatives (**5a-5f**), we perform 10 ns of MD simulation followed by calculation of binding free energy using MMGBSA and MMPBSA [44, 45]. Energy contribution of individual amino acids in the binding site was also determined.

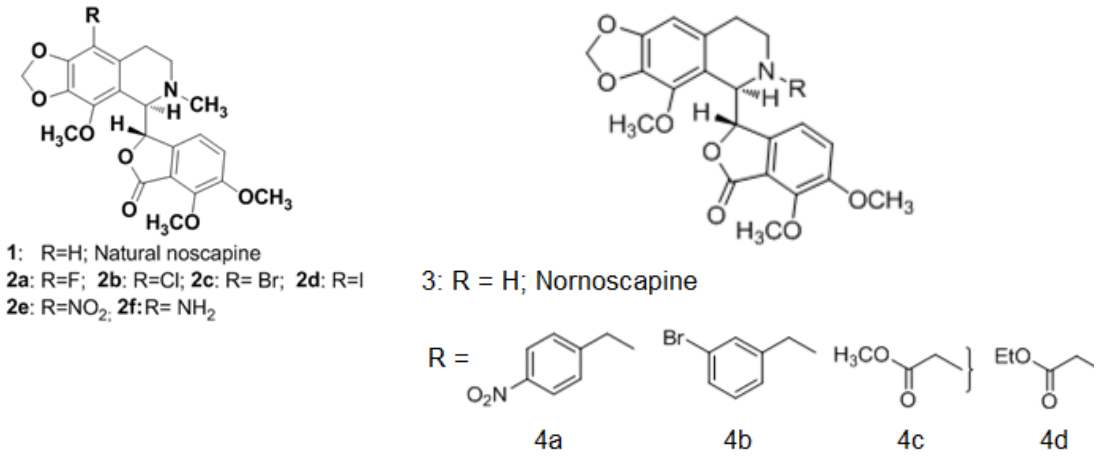

Figure 10. Molecular structure of previously reported Noscapinoids used in the training set.

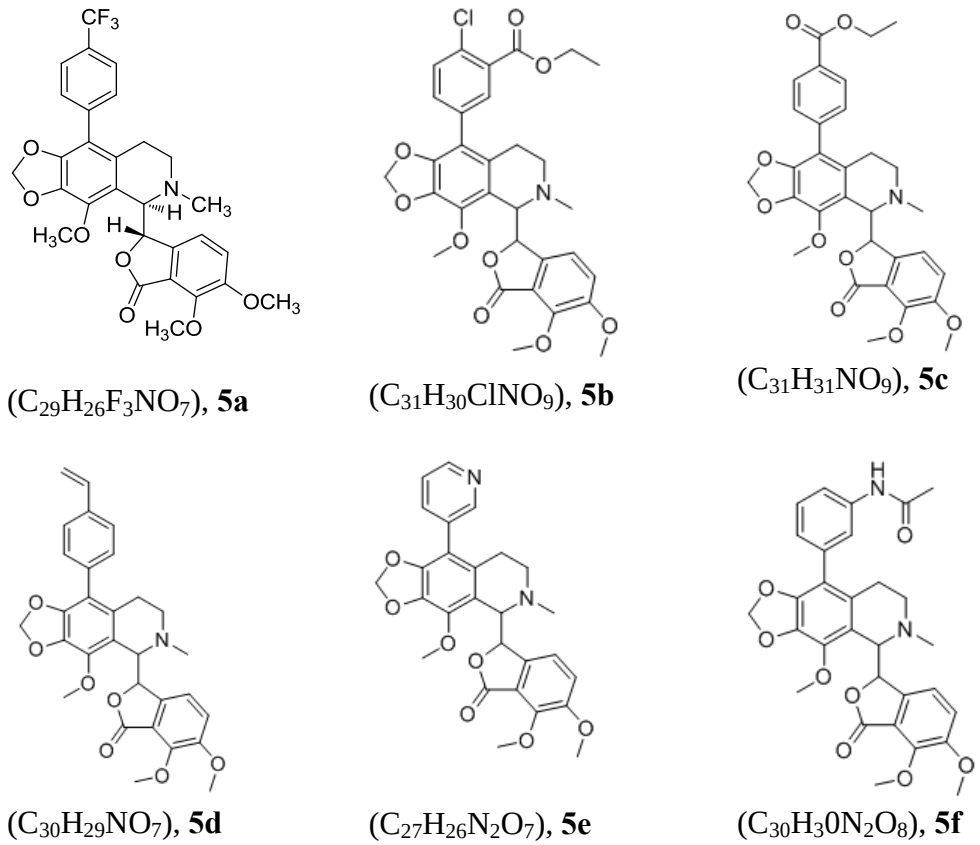

Figure 11. Molecular structure of newly designed Noscapinoids, **5a-5f** in this study.

Inspired by the computational prediction, these analogues were chemically synthesized for further experimental evaluation.

General procedure for the chemical synthesis of 5a-f analogues

In a Oven dried Round bottom flask 9-bromonoscapine 200 mg (0.4072 mmoles), Boronic acid (0.8145 mmoles), $Pd(PPh_3)_4$ (0.04886 mmoles), Sodium bicarbonate (0.8145.mmoles) were

taken. 10mL of ethanol, toluene(1:1) mixture was added. Reaction mixture was heated at 120 ^{0}C for 48 hours. Reaction mixture was cooled to room temperature solvents were removed at reduced pressure extracted with Dichloromethane (3x25mL) dried over anhydrous sodium sulphate concentrated to give crude product which is purified by column chromatography (25% EtOAc in Hexanes) to give pure products as white solids.

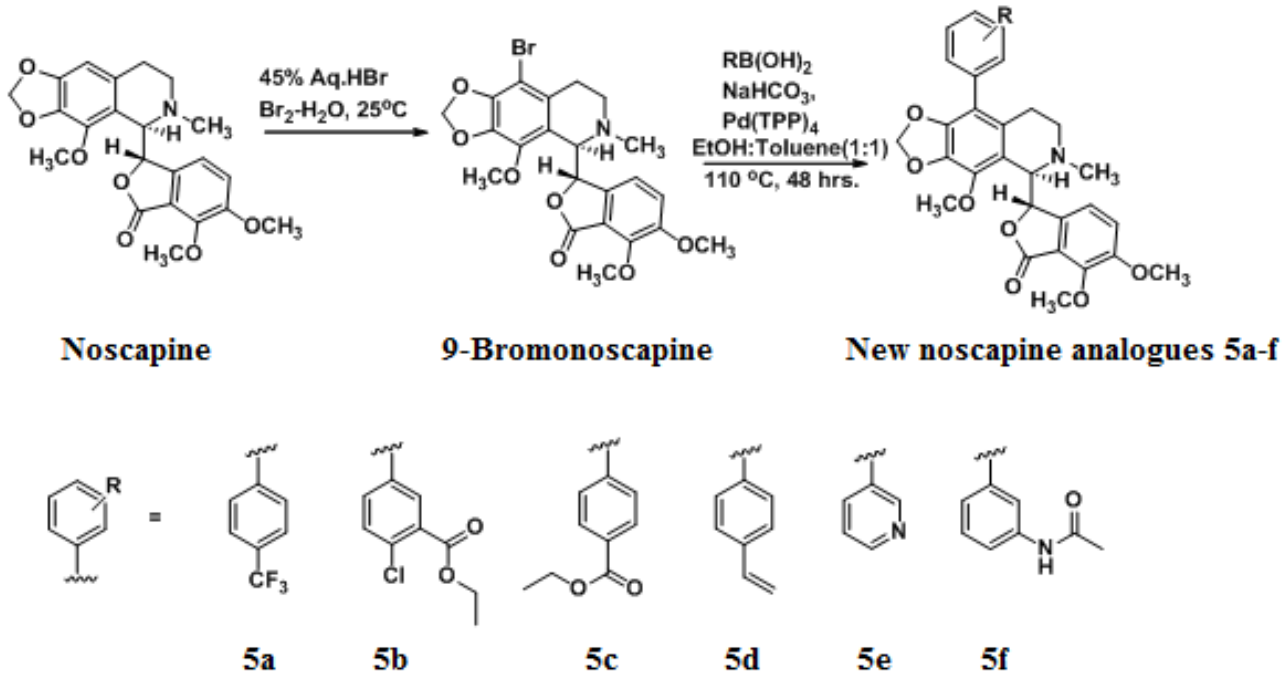

Synthetic scheme of synthesis of 9-arylnoscapine analogues.

6,7-dimethoxy-3-(4-methoxy-6-methyl-9-(4-(trifluoromethyl)phenyl)-5,6,7,8-tetrahydro-[1,3]dioxolo[4,5-g]isoquinolin-5-yl)isobenzofuran-1(3H)-one (5a).

Yield:65%; MP:135°C.^{1}H NMR ($CDCl_3$, 300MHz) δ 7.60-7.40(m, 4H), 6.97(d, J=8.12, 4H), 6.05(d, J=8.30, 1H), 6.02(d, J=1.32, 1H), 5.93(d, J=1.32Hz, 1H), 5.44(d, J=4.15, 1H), 4.46(d, J=4.34, 1H), 4.14(s, 3H), 4.10(s, 3H), 3.89(s, 3H), 2.65-2.51(m, 4H), 2.20-2.00(m, 2H), 1.70-1.56(m, 1H). ^{13}C NMR ($CDCl_3$, 75MHz) δ 167.9, 152.4, 147.5, 146.0, 140.5, 140.0, 134.9, 133.2, 128.7, 126.7, 126.6, 124.1, 120.5, 118.1, 117.2, 114.7, 100.9, 81.8, 62.2, 61.0, 59.5, 56.5, 50.7, 46.7, 29.6, 27.2. IR(KBr) 3413, 2948, 1765, 1614, 1497, 1422, 1237, 1158, 1120, 1039, 946, 806, 732, 701 cm^{-1}.MS(EI) m/z 580 $(M+Na)^+$; HRMS(ESI) Calcd for $C_{29}H_{26}NO_7F_3Na(M+Na)^+$: 580.1559, found: 580.1568

Ethyl 2-chloro-5-(5-(4,5-dimethoxy-3-oxo-1,3- dihydroisobenzofuran-1-yl) - 4-methoxy-6-methyl-5,6,7,8-tetrahydro-[1,3]dioxolo[4,5-g]isoquinolin-9-zl)benzoate (5b).

Yield:70%; MP:152°C.^{1}H NMR ($CDCl_3$, 300MHz) δ 7.64(d, J=2.07Hz, 1H), 7.454(d, J=8.30, 1H), 7.34-7.27(m, 1H), 7.02(d,J=8.12, 1H), 6.16-6.05(d, J=7.93Hz, 1H), 6.00(s, J= 1H), 5.92(s, 1H),

4.49-4.34(m 3H), 4.10(s, 6H), 3.91(s, 3H), 2.72-2.53(m, 4H), 2.26-2.09(m, 2H), 1.66(s, 1H), 1.42(t, J=7.17Hz, 3H), ^{13}C NMR ($CDCl_3$, 75MHz) 167.9, 165.6, 152.3, 147.6, 146.0, 140.8, 140.1, 133.7, 132.9, 132.5, 130.8, 130.5, 130.3, 120.4, 118.1, 117.7, 117.6, 114.1, 100.9, 81.8, 62.9, 61.6, 61.0, 59.5, 56.8, 50.5, 46.6, 26.9, 14.1. IR(KBr) 3418, 2922, 2853, 2795, 1756, 1633, 1597, 1498, 1363, 1274, 1159, 1036, 940, 813, 728, 506cm^{-1}. MS (ESI) m/z 618 $(M+Na)^+$; HRMS(ESI) Calcd for $C_{31}H_{30}NO_9ClNa$ $(M+Na)^+$: 618.1506, found : 618.1476

Ethyl 4-(5-(4,5-dimethoxy-3-oxo-1,3-dihydro isobenzofuran-1-yl)-4-methoxy-6-methyl-5,6,7,8-tetrahydro-[1,3]dioxolo[4,5-g]isoquinolin-9-yl)benzoate (5C)

Yield:67%; MP: 143°C .1H NMR (CDCl3, 300MHz) δ 8.09(d, J=8.49Hz, 2H), 7.33(d, J=8.30Hz, 2H), 7.03(d, J=8.30Hz, 1H), 6.16(d, J=8.12Hz, 1H), 6.00(d, J=1.32, 1H), 5.93(d, J=1.32Hz, 1H), 5.54(d, J=4.15Hz, 1H), 4.49(d, J=4.34 1H), 4.40(q, J=7.17, 2H), 4.12(s 3H), 4.11(s 3H), 3.91(s, 3H), 2.67-2.52(m, 4H), 2.27-2.11(m, 2H), 1.76-1.65(m, 1H), 1.41(t, J=7.17, 3H).13C NMR (CDCl3, 75MHz) δ 167.9, 166.2, 152.3, 147.7, 146.0, 140.9, 140.0, 138.9, 133.7, 130.6, 130.0, 129.3, 120.5, 118.1, 117.7, 115.4, 100.9, 81.8, 62.2, 61.1, 60.9, 59.5, 56.9, 56.7, 46.7, 27.0, 14.3 .IR(KBr) 3413, 2915, 1767, 1697, 1616, 1498, 1464, 1443, 1381, 1306, 1262, 1165, 1088, 1034, 1012, 821, 621cm-1.MS(ESI) m/z 584 (M+Na)+; HRMS (ESI) Calcd for C31H31NO9Na (M+Na)+: 584.1896, found: 584.1881.

6,7-dimethoxy-3-(4-methoxy-6-methyl-9-(4-vinylphenyl)-5,6,7,8-tetrahydro-[1,3]dioxolo[4,5-g]isoquinolin-5-yl)isobenzofuran-1(3H)-one (5d)

Yield:60%; MP:120°C.1H NMR (CDCl3, 300 MHz) δ 7.40(d, J=8.20Hz, (d, J=8.24, 2H), 7.17(d, J=8.04, 2H), 6.97(d, J=8.14, 1H), 6.74-6.66(dd, J=10.86, 17.45 1H), 6.10(s, 1H), 5.98(s, 1H), 5.91(s, 1H), 5.74(d, J=17.55, 1H), 5.48(s, 1H), 5.25(d, J= 4.15Hz, 1H), 4.47(s, 1H), 4.10(s, 1H), 3.90(s, 3H), 2.66-2.54(m, 4H), 2.27-2.13(m, 2H), 1.77-1.64(m, 1H).13C NMR (75 MHz, CDCl3) δ 157.9, 152.2, 147.7, 146.0, 143.6, 140.9, 139.6, 136.7, 133.7, 133.5, 130.7, 130.1, 126.0, 120.4, 117.8, 116.1, 114.2, 100.8, 81.9, 62.3, 61.1, 59.5, 56.9, 50.8, 46.6, 27.0, 23.2, 29.6. MS(ESI) m/z 538(M+Na)+: HRMS(ESI) Calcd for C30H29NO7Na(M+Na)+: 538.1841, found: 538.1848.

6,7-dimethoxy-3-(4-methoxy-6-methyl-9-(pyridin-3-yl)-5,6,7,8-tetrahydro-[1,3]dioxolo[4,5-g]isoquinolin-5-yl)isobenzofuran-1(3H)-one (5e)

Yield:62%; MP:193°C.^{1}H NMR ($CDCl_3$, 500MHz) δ 8.52(s 1H), 8.43(s, 1H) 7.56(d, J=7.6Hz, 1H), 7.30(t, J=6.6Hz, 1H), 6.12(d, J=7.6Hz,1H), 5.99(s,1H), 5.92(s, 1H), 5.43(d, J=4.7Hz,1H), 4.43(d, J=4.7Hz,1H).4.11(s, 3H), 4.08(s, 3H), 3.88(s, 3H),2.67-2.60(m,1H), 2.55(s,3H), 2.22-2.14(m, 2H), 1.79-1.69(m,1H).IR C13 NMR 167.9, 152.3, 150.7, 147.6, 146.4, 140.7, 140.2, 137.3, 133.7, 130.7, 123.1, 120.4, 118.2, 117.5, 100.9, 81.8, 62.2, 61.0, 59.4, 56.8, 50.6, 46.6, 26.8.(KBr)

3412, 2938, 1756, 1637, 1497, 1445, 1273, 1082, 1032, 943, 815, 714, cm^{-1}. MS(ESI) m/z: 513 $(M+Na)^+$; HRMS (ESI) Calcd for $C_{27}H_{26}N_2O_7Na(M+Na)^+$: 513.1637, found: 513.1615

N-(3-(5-(4,5-dimethoxy-3-oxo-1,3-dihydroisobenzofuran-1-yl)-4-methoxy-6-methyl-5,6,7,8-tetrahydro-[1,3]dioxolo[4,5-g]isoquinolin-9-yl)phenyl)acetamide (5f)

Yield:55%; MP:240°C.^{1}H NMR ($CDCl_3$, 300MHz) δ 7.68(s, 1H), 7.46-7.28(m, 1H), 7.25-7.12(d, J=8.30 1H), 7.07-6.93(d, J=7.17, 1H)6.23-6.10(d, J=8.30Hz, 1H), 5.98(s, 1H), 5.91(s, 1H), 5.54(d, J=3.96Hz, 1H).4.50(d J=3.96, 1H), 4.10(s, 6H), 3.94(s, 3H0, 2.54(s, 5H), 2.27-2.10(m, 4H), 1.77-1.60(m, 1H) ^{13}C NMR ($CDCl_3$, 75MHz) δ 168.4, 152.2, 147.3, 145.9, 140.6, 139.5, 138.2, 134.9, 133.6, 130.8, 128.5, 1255, 121.3, 120.2, 118.3, 117.9, 117.6, 116.3, 100.8, 82.1, 62.1, 61.0, 59.4, 56.4, 50.8, 46.7, 27.0, 24.4. IR (KBr) 3329, 2920, 2791, 1739, 1682, 1586, 1548,1503, 1384, 1274, 1086, 1037,797, 620 cm^{-1}. MS(ESI) m/z 569 $(M+Na)^+$; HRMS (ESI) Calcd for $C_{30}H_{30}N_2O_8Na(M+Na)^+$: 569.1899, found: 569.1920.

Cell cytotoxicity of these analogues was determined in cancer cell lines like MCF-7, HeLa and A549 using MTS assay. The effect of these derivatives in the cell cycle progression was studied using MCF-7 cell line based on flow cytometry analysis. Binding affinity of these analogues measured in terms of dissociation constant (K_d value) with tubulin was determined using tubulin binding assay. The representative molecule (**5e)** which showed better activity was used for toxicity analysis in Sprague–Dawley rats. All experimental protocols involved in this study were approved by Institutional Animal Ethics Committee, DIHAR, DRDO and followed by the guidelines of "Committee for the Purpose of Control and Supervision of Experiments on Animals" of Govt. of India. Adult male and female Sprague–Dawley rats (n = 30) used in this study were divided into six experimental groups (5 rats/group) for the study. Group 1 & Group 2 served as control for male and female rats respectively. Two oral doses of compound **5e** such as 25 mg/kg body weight (for sub-chronic Group 3(male) & 4(female)) and 50 mg/kg body weight (for acute Group 5(male) & 6(female)) were administrated for toxicological evaluation. The rats in the sub-chronic groups were fed with the drug daily upto 28 days, whereas the rats in the acute group were fed only once. At the end of the experiment, animals in group1-4 were sacrificed on day 28, whereas animals in group 5 and 6 were sacrificed on day 14. Blood samples were collected directly from the heart for haematology and clinical biochemistry on the day of sacrifice. For histological studies the animals were sacrificed using perfusion. The vital organs such as brain, duodenum, liver, lungs, kidney, heart and spleen were removed, postfixed in 4% paraformaldehyde in PBS and further processed for histopathological analysis[47,48].

Results and discussion

Availability of structure activity data of some Noscapinoids allow us to develop a reasonable predictive model for the screening of novel Noscapinoids with improved binding affinity in comparison to lead molecule, Noscapine. All these molecules were docked into the Noscapinoid binding site [24] using Glide XP (extra precision) and their docked complexes were used to calculate various energy parameters using LIE-SGB method to develop the following predictive model. The predicted ΔG_{bind} of the training set molecules based on the predictive model are very close to the experimental ΔG_{bind} (root mean square error was 0.288 kcal/mol) (Table 12). The quality of the fit can also be judged by the value of the squared correlation coefficient (R^2) and analysis of variance (F-value).

$$\Delta G_{bind} = 0.0762\langle U_{vdw}\rangle - 0.00965\langle U_{elec}\rangle - 0.520\langle U_{cav}\rangle \quad (2)$$

$$(n = 12, R^2 = 0.776, s = 0.26, F = 1969.8, P = 0.000, PRESS = 1.243)$$

Because of high predictability, the LIE model was used to predict the ΔG_{bind} of the newly designed Noscapinoids. Among the library of newly designed Noscapinoids, some of the derivatives (**5a-5f)** (Figure 11) which showed improved predicted binding affinity (ranging from -5.568 to -5.970 kcal/mol) were finally selected for further analysis (Table 13). These newly designed Noscapinoids, **5a-5f,** also showed better docking scores ranging from -8.466 kcal/mol to -6.085 kcal/mol than the parent compound, Noscapine (-5.505 kcal/mol) (Table 13).

Table 12. Molecular docking results (Glide XP) as well as calculated energies based on LIE-SGB model of training set Noscapine derivatives: van der Waals (vdw), electrostatic (elec), cavity (cav), predicted and experimental binding free energy (ΔG_{bind}).

Ligand	Glide XP_{score} (kcal/mol)	$\langle U_{vdw}\rangle$ (kcal/mol)	$\langle U_{elec}\rangle$ (kcal/mol)	$\langle U_{cav}\rangle$ (kcal/mol)	K_d value (μM)	Experimental ΔG_{bind} (kcal/mol)	Predicted ΔGbind (kcal/mol)
1	-5.505	-52.06	43.32	1.720	152 ± 1.0	-5.214	-5.194
2a	-5.684	-47.65	119.8	1.432	81 ± 8.0	-5.587	-5.951
2b	-6.152	-59.54	68.27	2.12	40 ± 8.0	-6.006	-6.063
2c	-6.437	-58.92	87.54	1.59	54 ± 9.1	-5.827	-6.355
2d	-5.463	-58.13	83.35	1.059	22 ± 4.0	-6.360	-5.755
2e	-6.228	-57.71	129.2	1.846	86 ± 6.0	-5.551	-5.835
2f	-5.279	-59.48	63.57	1.324	14 ± 1.0	-6.628	-6.540
3	-5.639	-53.28	87.36	0.823	68 ± 0.7	-5.691	-5.416
4a	-6.087	-63.42	41.26	0.824	91 ± 8.0	-5.518	-5.394
4b	-7.252	-62.62	76.32	1.232	38 ± 4.0	-6.036	-5.795
4c	-5.712	-61.82	41.32	0.698	79 ± 8.0	-5.602	-5.128
4d	-5.402	-56.95	7.851	0.756	228 ± 10.0	-4.973	-5.078

$\langle U_{vdw}\rangle$, $\langle U_{elec}\rangle$ and $\langle U_{cav}\rangle$ energy terms represents the ensemble average energy terms calculated as the difference between bound and free state of the ligands and its environment. Experimental ΔG_{bind} was calculated from the dissociation constant (K_d value) using the relationship: $\Delta G_{bind} = RT \ln K_d$ where T = 298 K and R = 0.00199 (kcal/mol.K). Predicted ΔG_{bind} was calculated using (LIE-SGB empirical equation**:** $\Delta G_{bind} = 0.0762 \langle U_{vdw}\rangle - 0.00965 \langle U_{elec}\rangle - 0.520 \langle U_{cav}\rangle$.

Table 13. Molecular docking results (Glide XP) as well as calculated energies based on LIE-SGB model of newly designed Noscapinoids (**5a-5f**): van der Waals (vdw), electrostatic (elec), cavity (cav), predicted and experimental binding free energy (ΔG_{bind}).

Ligand	Glide XP_{score} (kcal/mol)	$<U_{vdw}>$ (kcal/mol)	$<U_{elec}>$ (kcal/mol)	$<U_{cav}>$ (kcal/mol)	Predicted ΔG_{bind} (kcal/mol)	K_d value (μM)	Experimental ΔG_{bind} (kcal/mol)
5a	-6.085	-60.57	41.82	1.05	-5.568	126 ±5.0	-5.325
5b	-6.397	-60.68	50.47	1.62	-5.954	-	-
5c	-6.833	-59.44	53.78	1.23	-5.689	107 ±5.0	-5.422
5d	-6.845	-63.89	63.01	0.49	-5.732	71 ±4.0	-5.665
5e	-7.717	-63.21	61.54	1.07	-5.965	68 ±6.0	-5.691
5f	-8.466	-67.39	44.45	0.78	-5.970	-	-

Experimental ΔG_{bind} was calculated from the dissociation constant (K_d value) using the relationship: $\Delta G_{bind} = RT \ln K_d$ where T = 298 K and R = 0.00199 (kcal/mol.K). Predicted ΔG_{bind} was calculated using LIE-SGB empirical equation: $\Delta G_{bind} = 0.0762 <U_{vdw}> - 0.00965 <U_{elec}> - 0.520 <U_{cav}>$

To further refine binding free energy score and to calculate the energy contribution of individual amino acids of tubulin with newly designed Noscapinoids, **5a-5f**, MM-PBSA and MM-GBSA methods have been used. Energy values were calculated as the average value out of 1000 snapshots generated from the last 2 ns of the MD trajectory for each tubulin-Noscapinoid complex. The total calculated binding free energy (ΔG_{bind}) of the Noscapinoids, **5a-5f** with tubulin and their detailed energy contributions calculated according to the MM-PBSA and MM-GBSA approaches are summarized in Table 14. The calculated ΔG_{bind} based on both the methods, MM-PBSA and MM-GBSA, indicate that all the newly designed Noscapinoids bind to tubulin with a greater affinity in the following order of magnitude: 5f > 5e > 5d > 5c > 5b > 5a. All the Noscapinoids, **5a-5f** are well accommodated into the binding site, at the interface between α- and β- tubulin (Figure 12). However, their binding modes inside the binding cavity are distinct (Figure 13). The differences in binding modes of these Noscapinoids, **5a-5f** are not only due to various substitutions of functional groups in the scaffold structure but also because of differential contribution in binding free energy of amino acids involved in the interactions. Binding free energy of individual amino acid involved in the interaction with these ligands was calculated based on MM-GBSA calculation and plotted in Figure 14. The analysis reveals that Leu253 is consistently important contributor to the binding energy among all the Noscapinoids. Inspired by our computational findings, we have made attempt to synthesize these compounds, **5a-f** to further evaluate their experimental activities.

Table 14: Change in binding free energy and its components (kcal/mol) for the Noscapine derivatives **5a-5f** binding with tubulin.

Energy components (kcal/mol)	5a	5b	5c	5d	5e	5f
ΔE_{ele}	-320.1	-318.6	-318.2	-314.7	-42.95	-340.7
ΔE_{vdw}	-66.03	-69.19	-74.87	-68.41	-51.42	-72.01
ΔE_{gas}	-386.2	-387.8	-393.0	-383.1	-94.36	-412.7
$\Delta G_{sol\text{-}np}$	-7.593	-7.906	-8.629	-7.070	-5.953	-7.857
ΔG_{PB}	356.2	357.7	362.6	345.8	56.82	375.5
$\Delta G_{solv,PB}$	351.1	351.8	356.5	340.9	52.02	370.3
$\Delta G_{ele,PB}$	36.08	39.11	44.41	31.11	13.87	34.79
$\Delta G_{bind,\ PB}$	**-35.12**	**-35.94**	**-36.52**	**-42.22**	**-42.34**	**-42.45**
ΔG_{GB}	350.9	349.7	352.0	342.1	52.04	370.2
$\Delta G_{solv,GB}$	343.3	341.8	343.4	335.1	46.09	362.3
$\Delta G_{ele,\ GB}$	30.77	31.08	33.84	27.43	9.091	29.44
$\Delta G_{bind,\ GB}$	**-42.85**	**-46.00**	**-49.64**	**-48.02**	**-48.27**	**-50.42**

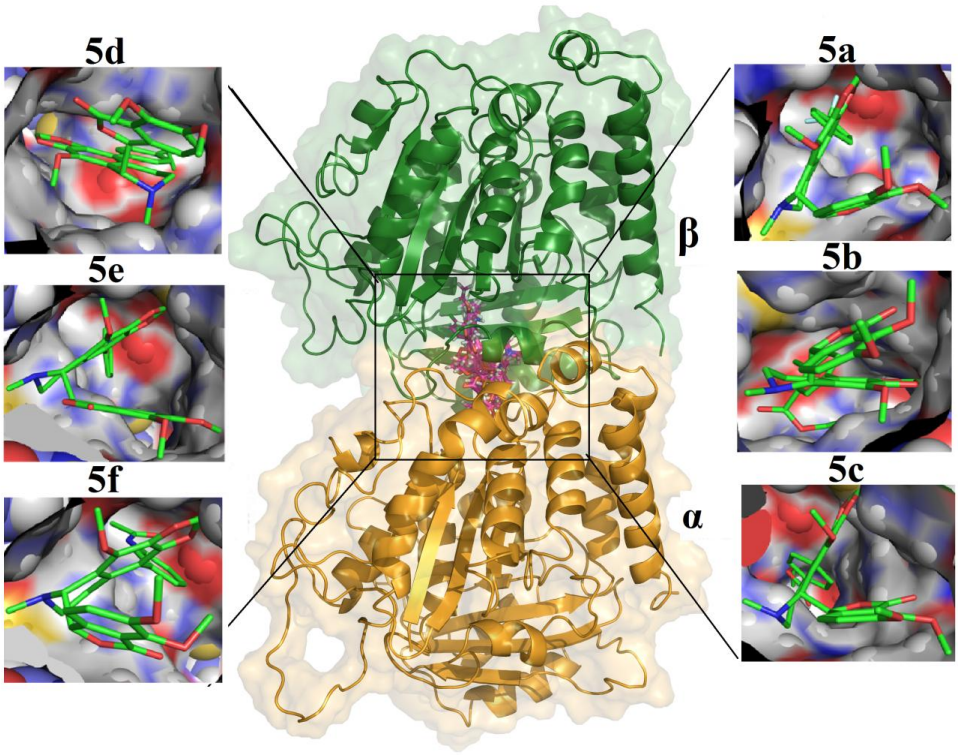

Figure 12. The newly designed Noscapinoids **5a-5f** are well accommodated in the Noscapinoid binding site at the interface between α- and β- tubulin. Snapshot of the ligands **5a-f** are obtained from the MM-GBSA calculation. The binding site is represented as Macromodel surface according to residue charge (electropositive charge, blue; neutral, yellow and electronegative charge, red) as implemented in Pymol.

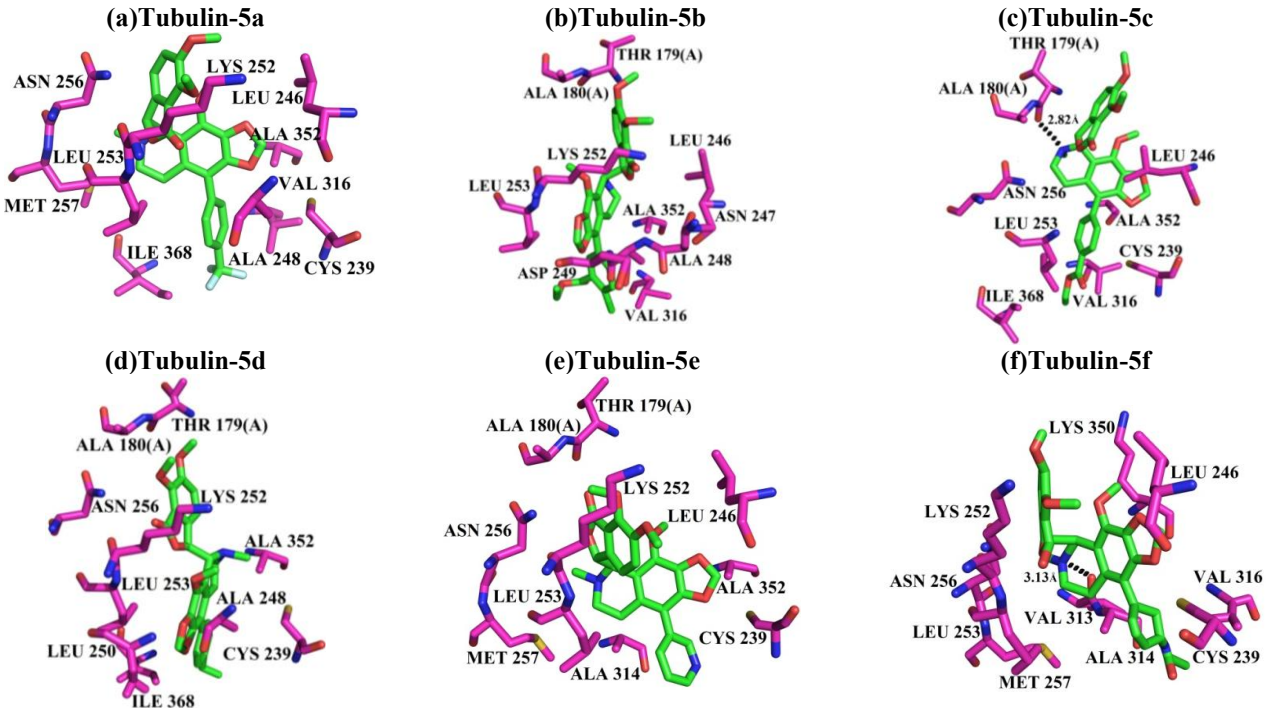

Figure 13. Typical snapshot of the binding mode of Noscapinoids **5a-5f** with tubulin. The hydrogen bonds formed (if any) are represented as dotted lines. The Noscapinoid **5c** forms one hydrogen bond with Thr179 of the α chain. The nitrogen atom N1 of the upper isoquinalone ring hydrogen bonds with oxygen atom of Thr179 with a distance of 2.82 Å .The Noscapinoid **5f** forms one hydrogen bond with Val313 of the β chain. The nitrogen atom N1 of the upper isoquinalone ring hydrogen bonds with oxygen atom of Val313 with a distance of 3.13 Å. The other Noscapinoids however do not involve any hydrogen bonds. The difference in binding modes of these Noscapinoids is due to various substitutions in the scaffold structure.

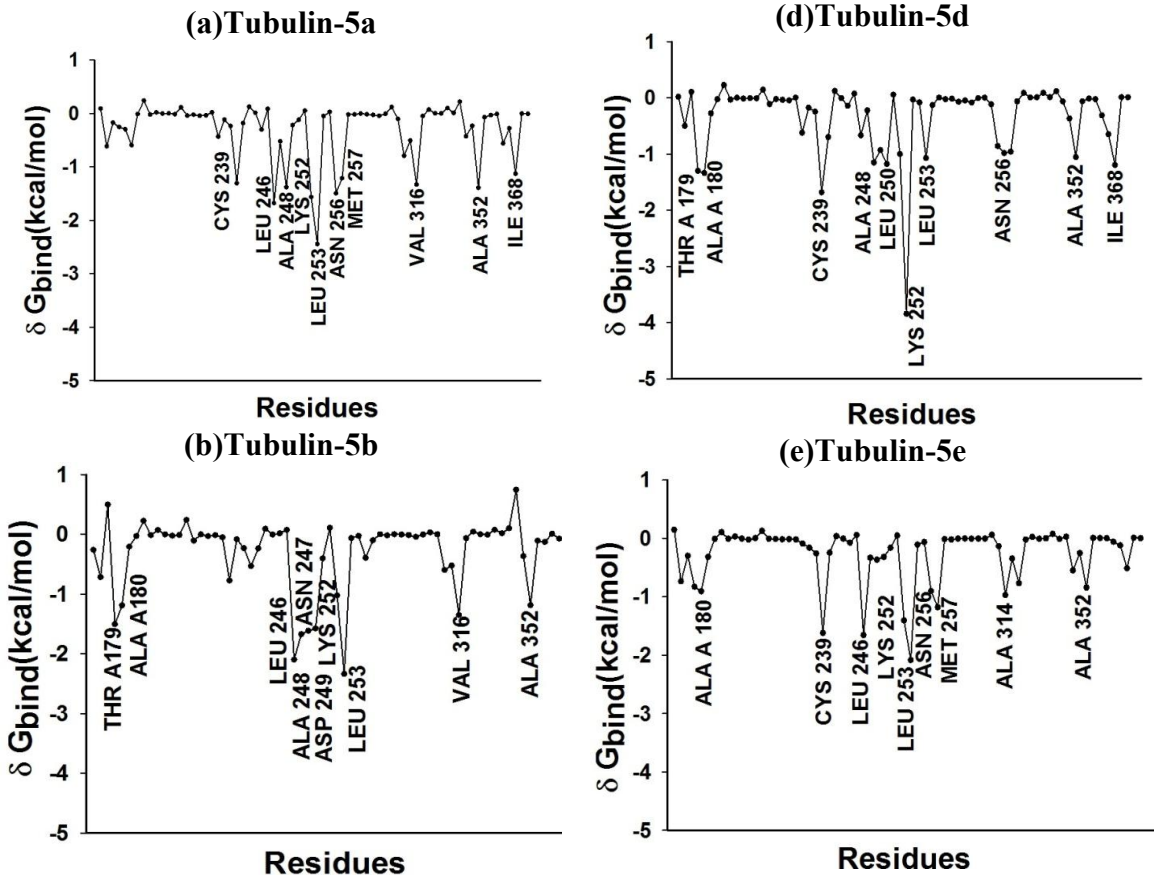

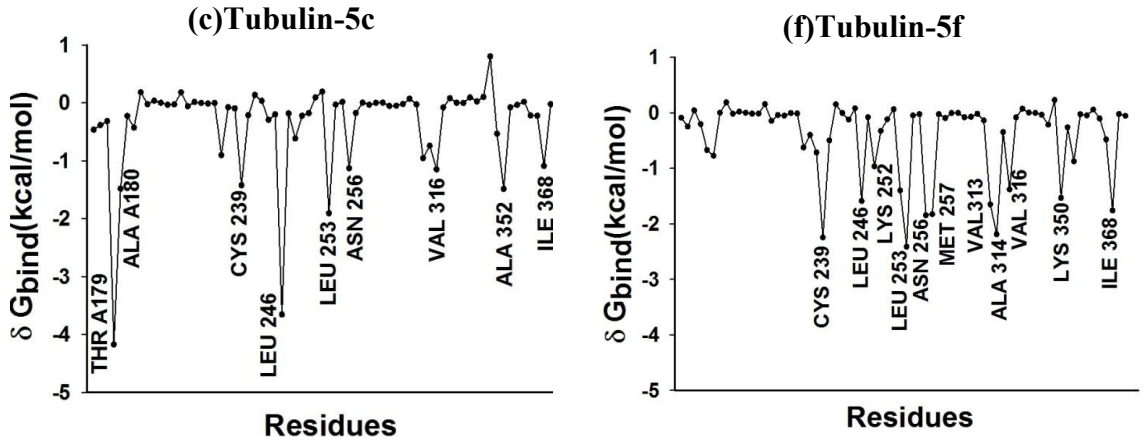

Figure 14: Total binding energy (δG_{bind}) contribution on per residue basis in tubulin-drug complexes. The residues within 12 Å of the docked ligand were only considered.

For experimental evaluation all the compounds including Noscapine were evaluated for their anti-proliferative activity in three human cancer cell lines; human breast adenocarcinoma cells (MCF-7), human cervix cancer cells (HeLa) and human lung adenocarcinoma cells (A549). The IC_{50} values for the test compounds **5a-5f** for these three cell lines are collected in Table 15. All the compounds possess potent cytotoxic activity. Especially three compounds **5b, 5e** and **5f** showed better activity among all the three cell lines. The cell cycle analysis in MCF-7 further revealed that Noscapinoids 5a-5f alter the cell cycle profile and cause mitotic arrest at G2/M phase more actively than Noscapine (Figure 15).

Table 15. IC_{50} values (a drug concentration required to achieve a 50% inhibition of cellular proliferation) of Noscapine derivatives **5a-5f** for various cancer cell types[a].

Noscapine analogue	HeLa (µM)	A549 (µM)	MCF-7 (µM)
5a	22.8 ± 2.8	57.3 ± 3.9	41.3 ± 2.4
5b	9.0 ± 1.5	33.8 ± 3.5	18.8 ± 2.7
5c	21.2 ± 3.7	53.1 ± 3.7	40.7 ± 3.3
5d	20.3 ± 2.5	42.7 ± 2.9	34.3 ± 2.5
5e	8.9 ± 1.7	31.6 ± 2.6	16.6 ± 2.9
5f	6.7 ± 1.4	30.6 ± 2.5	13.8 ± 2.5
Noscapine	24.0 ± 2.9	62.9 ± 4.6	42.3 ± 2.7

[a] Cancer cells used in the assay namely, HeLa: human cervix cell line, A549: human lung adenocarcinoma epithelial cell line and MCF7: human breast epithelial cell line. Each value represents mean ± S.D. from three different experiments.

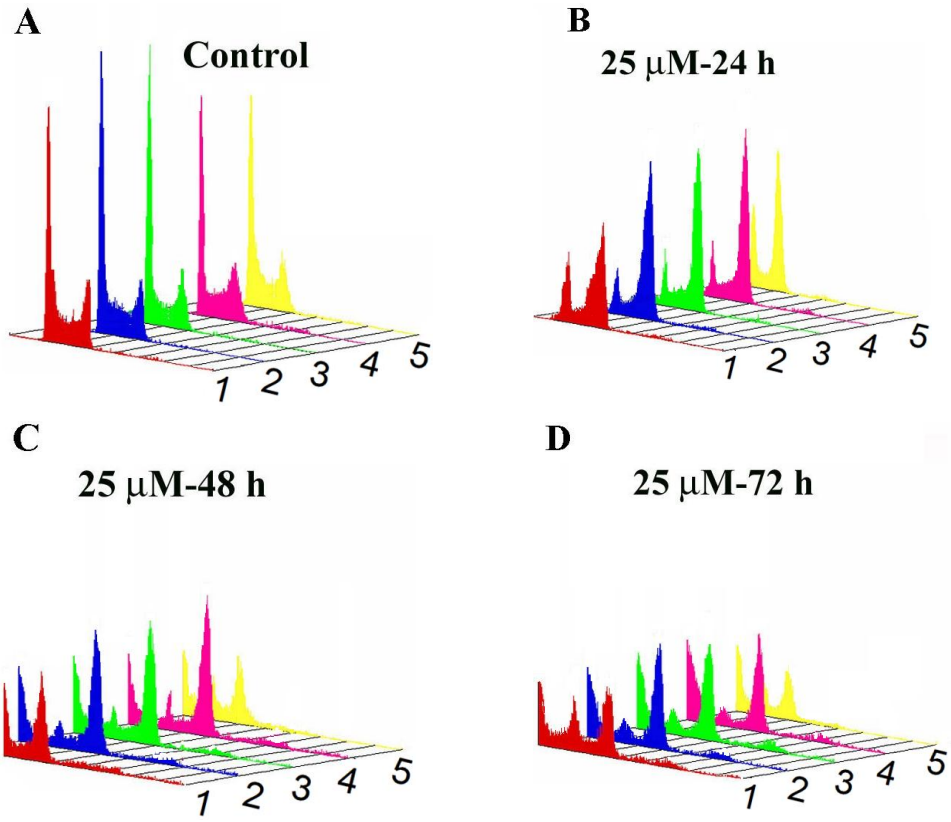

Figure 15. Noscapine analogs inhibit cell cycle progression at mitosis followed by the appearance of a characteristic hypodiploid (sub-G1) DNA peak, indicative of apoptosis. Panel A-D depict analyses of cell cycle distribution in a three-dimensional disposition as determined by flow cytometry in MCF-7 cells treated with 25 μM concentration of noscapine analogs (1: 5c, 2: 5d, 3: 5e, 4: 5f and 5: 5a) for 0, 24, 58 and 72 hours respectively.

Tubulin binding assay revealed higher binding affinity of the newly designed analogues, as suggested by dissociation constant (K_d) of 126 ± 5.0 μM for **5a**, 107 ± 5.0 μM for **5c**, 71 ± 4.0 μM for **5d**, and 68 ± 6.0 μM for **5e** binding to tubulin (Table 13, Figure 16) which is better than previously reported dissociation constant (K_d) of 152 ± 1.0 μM for Noscapine binding to tubulin [18]. The other two derivatives, **5b** and **5f** also showed potential binding to tubulin as indicated by the tryptophan quenching pattern, but we could not obtain reliable and reproducible K_d values due to a non-linear nature of the quenching pattern and higher absorbance of the compounds at the excitation and emission wavelengths (data not shown). Experimental ΔG_{bind} of these compounds was calculated from the K_d value using the relationship: $\Delta G_{bind} = RT \ln K_d$ where T = 298 K and R = 0.00199 (kcal/mol.K). In fact, this experimentally determined value of ΔG_{bind} (Table 12 and 13) are in the blueprint of predicted value of ΔG_{bind} calculated based on LIE-SGB, MM-PBSA and MM-GBSA, suggesting that these methods are reasonably accurate in rational design of potent Noscapinoids.

All the above analysis revealed 5e and 5f to be the most potent of the currently designed analogues. Due to the unavailability of complete tubulin binding data for 5f, I have selected 5e for

further toxicological evaluation. To determine whether compound 5e treatment results in toxicities to normal tissues, the vital organs like liver, kidney, spleen, lung, heart, brain and duodenum of the animals were examined (Figure 17). Treatment of animals with compound 5e, daily 25 mg/kg and once 50mg/kg, fails to reveal any detectable pathological abnormalities in normal tissues that are active in normal cell proliferation. Also there was no significant difference in haematological and blood biochemical parameters between the treated and untreated groups (Figure 18(a-e)). Also during the dosage regimen no abnormal behaviour regarding food and water consumption and body weights was observed

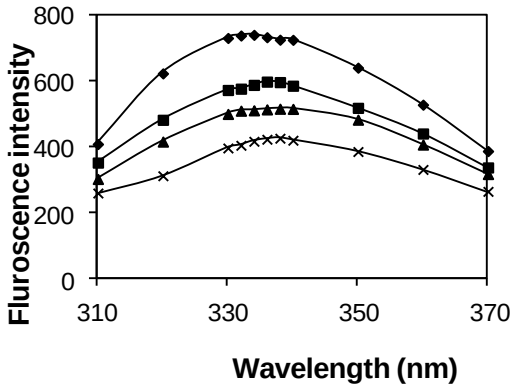

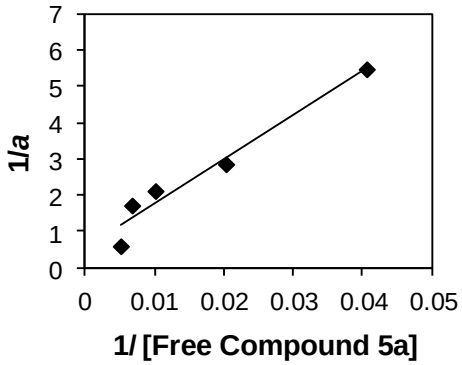

K_d = 126 ± 5.0 µM

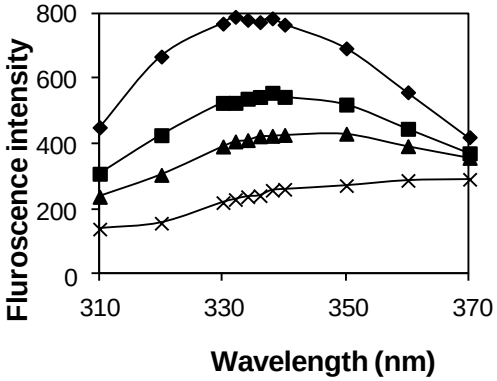

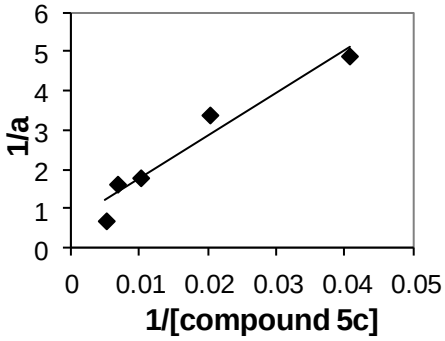

K_d = 107 ± 5.0 µM

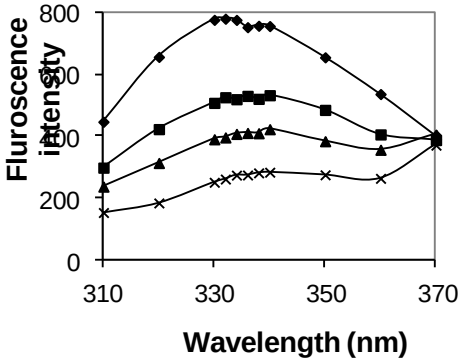

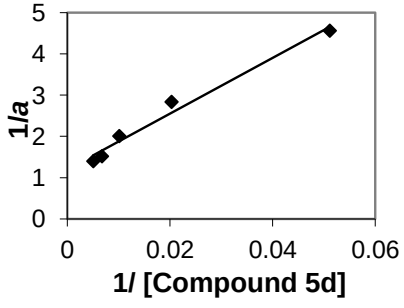

K_d = 71 ± 4.0 µM

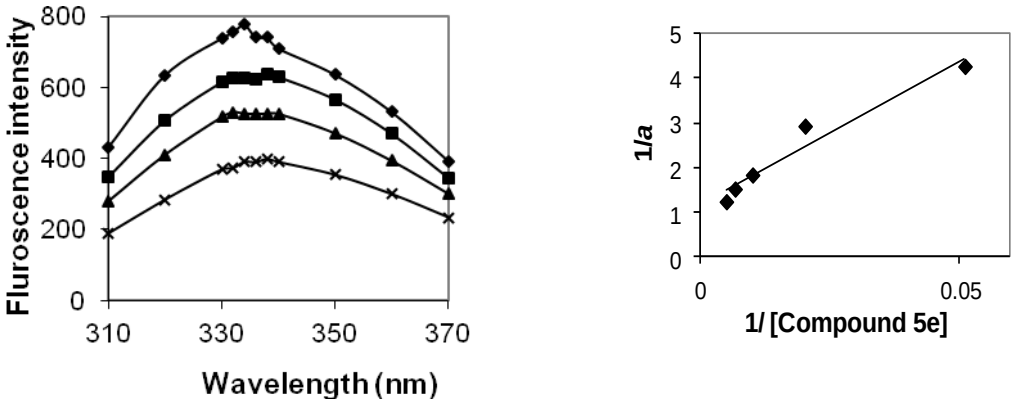

K_d = 68 ± 6.0 µM

Figure 16. The tubulin fluorescence emission intensity is quenched by noscapinoids 5a, 5c, 5d and 5e in a concentration dependent manner. The changes in fluorescence intensity is plotted as a function of concentration of drugs to calculate the K_d values.

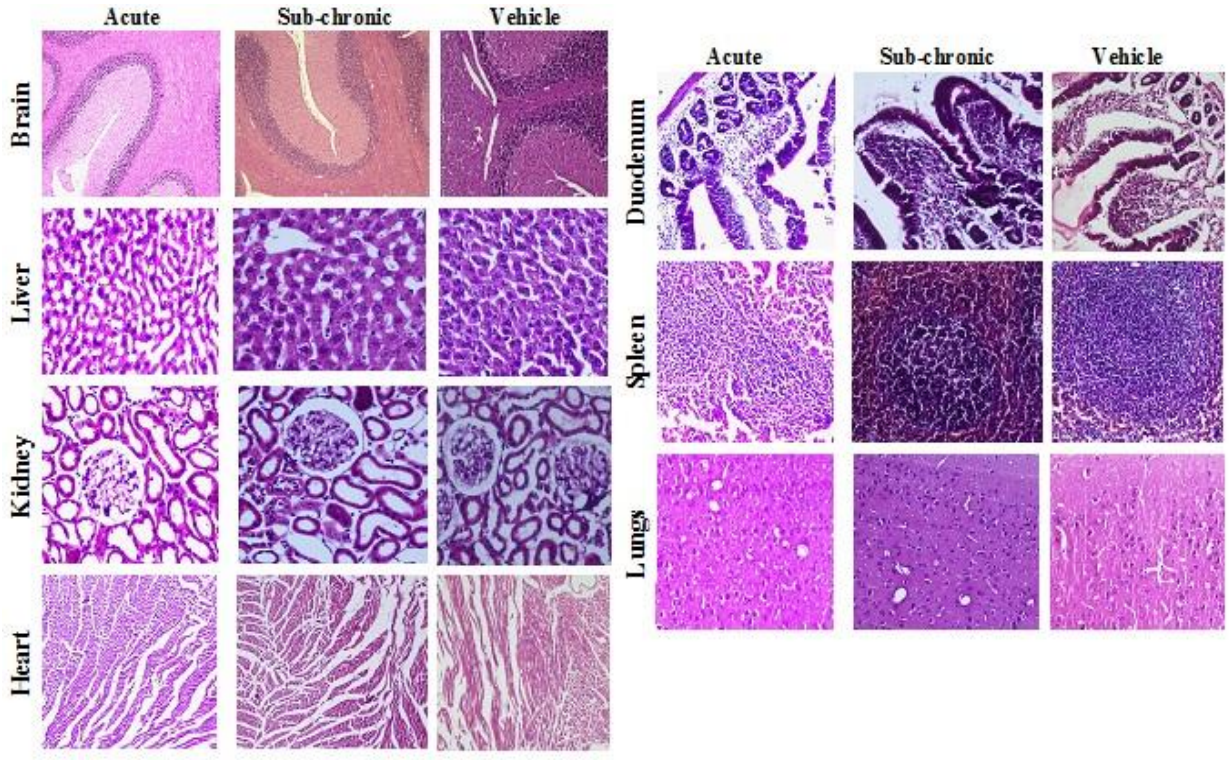

Figure 17. Panels represent H&E staining of paraffin-embedded 5 micron-thick sections of the liver, kidney, spleen, lung, heart, duodenum and brain at magnifications 200x and 400x. The liver showed normal hepatic lobular architecture. The kidneys revealed normal glomeruli, proximal and distal tubules, interstitium, and blood vessels. The splenic follicles and vascular sinusoids were indistinguishable between the 5e-treated and vehicle-treated control groups. The lung tissue showed normal alveoli and the heart muscle showed normal morphology among the two groups. Microsections of brain did not reveal any infracted areas. The cerebral cortex, gray and white matters appeared normal. The gut showed normal mucosa, submucosa and muscularis muco

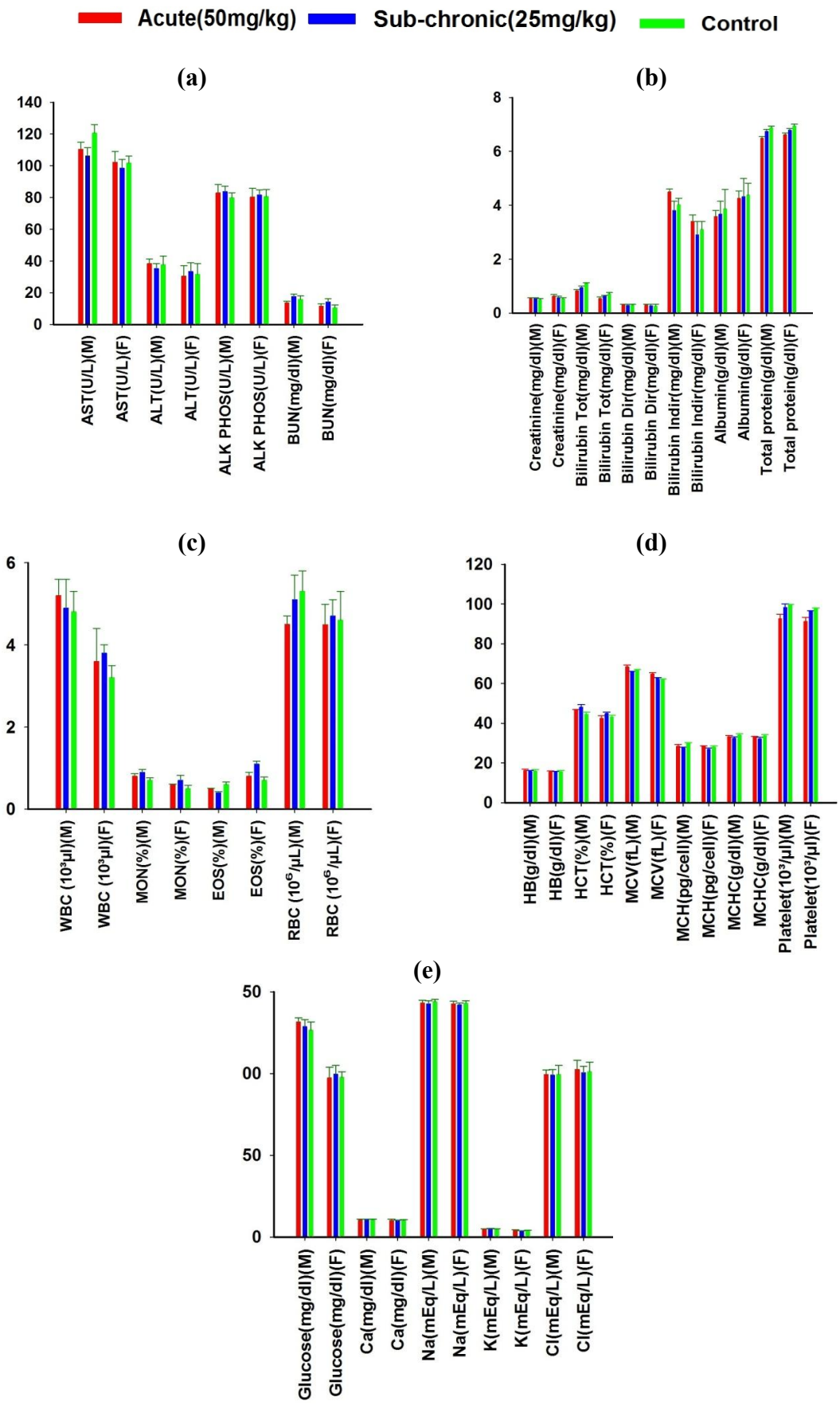

Figure 18. Organ functions(a) and (b) show undistinguishable profiles among the three groups ,Acute(50mg/kg), Sub-chronic(25mg/kg) and Control, for both male(M) and female(F) groups. No significant differences could be detected in the WBC count (WBC), monocytes (MON), eosinophils

(EOS), RBC count (RBC), haemoglobin concentration (HB),Hematocrit(HCT), mean corpuscular volume (MCV), mean corpuscular hemoglobin (MCH), mean corpuscular hemoglobin concentration (MCHC) and platelet count between treated and untreated groups, (c) and (d). Also there was no much difference in Serun Glucose, Serum Ca,NA,K, and Cl levels between the treated and untreated groups, (e).

Therefore, we believe that 5e is a safe and effective anti-cancer drug with a potential for the oral treatment cancer and holds great promise for further clinical studies.

Conclusion: Conclusively, we have provided computational methods that help in predicting the binding affinity of Noscapinoids with tubulin pertaining to screening of potent derivatives. Inspired by the improved calculated binding affinity by computational methods for the designed derivatives, we have chemically synthesized the designed derivatives. Most importantly, our results show that this series of Noscapine analogs increases its tubulin-binding activity and impacts its therapeutic potential for a variety of cancer cell types. Furthermore, the mechanism of cell death caused by these analogs is preserved, in that, like Noscapine, cell death is preceded by extensive mitotic arrest. In vivo toxicological evaluation of one of the compounds **5e** fail to reveal any toxicities in the vital organs like liver, kidney, spleen, lung, heart, brain and duodenum. Also there was no significant difference in hematological and blood biochemical parameters between the treated and untreated groups. Our data thus generate compelling evidence that these analogs indicate a great potential for further preclinical and clinical evaluation.

References

[1] Imran, Ali., Waseem, A. Wani and Kishwar Saleem. *Cancer Scenario in India with Future Perspectives.* Cancer Therapy, 8 pp 56-70. 2011.

[2] Margolis, R.L. and Wilson, L. Microtubule treadmills--possible molecular *machinery*. Nature, 293 pp 705-11. 1981.

[3] Margolis, R.L. and Wilson, L. *Microtubule treadmilling: what goes around comes around.* Bioessays, 20 pp 830-6. 1998.

[4] Jordan, M.A. and Wilson, L. *Microtubules as a target for anticancer drugs.* Nat Rev Cancer, 4 pp 253-65. 2004.

[5] Ngan, V.K., Bellman, K., Panda, D., *et al*. *Novel actions of the antitumor drugs vinflunine and vinorelbine on microtubules.* Cancer Res, 60 pp 5045-51. 2000.

[6] Schiff, P.B., Fant, J. and Horwitz, S.B. *Promotion of microtubule assembly in vitro by taxol.* Nature, 277 pp 665-7. 1979.

[7] Schiff, P.B. and Horwitz, S.B. *Taxol assembles tubulin in the absence of exogenous guanosine 5'-triphosphate or microtubule-associated proteins.* Biochemistry, 20 pp 3247-52. 1981.

[8] Rowinsky, E.K. *The development and clinical utility of the taxane class of antimicrotubule chemotherapy agents.* Annu Rev Med, 48 pp 353-74. 1997.

[9] Rowinsky, E.K., Eisenhauer, E.A., Chaudhry, V., et al. *Clinical toxicities encountered with paclitaxel (Taxol).* Semin Oncol, 20 pp 1-15. 1993.

[10] Ye, K., Ke, Y., Keshava, N., *et al*. *Opium alkaloid Noscapine is an antitumor agent that arrests metaphase and induces apoptosis in dividing cells.* Proc Natl Acad Sci USA, 95 pp 1601-6. 1998.

[11] Landen, J.W., Lang, R., McMahon, S.J. et al. *Noscapine alters microtubule dynamics in living cells and inhibits the progression of melanoma.* Cancer Res, 62 pp 4109-14. 2002.
[12] Zhou, J., Gupta, K., Yao, J. et al. *Paclitaxel-resistant human ovarian cancer cells undergo c-Jun NH2-terminal kinase-mediated apoptosis in response to Noscapine.* J Biol Chem, 277 pp 39777-85. 2002.
[13] Zhou, J., Panda, D., Landen, J.W., Wilson, L. and Joshi, H.C. *Minor alteration of microtubule dynamics causes loss of tension across kinetochore pairs and activates the spindle checkpoint*. Journal of Biological Chemistry 277 pp 17200-17208. 2002a.
[14] Ke, Y., Ye, K., Grossniklaus, H.E. et al. *Noscapine inhibits tumor growth with little toxicity to normal tissues or inhibition of immune responses.* Cancer Immunol Immunother, 49 pp 217-25. 2000.
[15] Aneja, R., Zhou, J., Vangapandu, S.N. et al. *Drug-resistant T-lymphoid tumors undergo apoptosis selectively in response to an antimicrotubule agent, EM011.* Blood, 107 pp 2486-92. 2006.
[16] Aneja, R., Kalia, V., Ahmed, R. and Joshi, H.C. (2007). *Nonimmunosuppressive chemotherapy: EM011-treated mice mount normal T-cell responses to an acute lymphocytic choriomeningitis virus infection.* Molecular Cancer Therapy, 6 pp 2891-2899.
[17] Aneja, R., Asress, S., Dhiman, N., Awasthi, A., Rida, P.C., Arora, S.K., Zhou, J., Glass, J.D. and Joshi, H.C. *Non-toxic melanoma therapy by a novel tubulin-binding agent.* International Journal of Cancer, 126 pp 256-265. 2010.
[18] Aneja, R., Vangapandu, S.N., Lopus, M., Chandra, R., Panda, D. and Joshi, H.C. *Development of a novel nitro-derivative of Noscapine for the potential treatment of drug-resistant ovarian cancer and T-cell lymphoma.* Molecular Pharmacology, 69 pp 1801-1809. 2006a.
[19] Aneja, R., Vangapandu, S.N., Lopus, M., Viswesarappa, V.G., Dhiman, N., Verma, A., Chandra, R., Panda, D. and Joshi, H.C. *Synthesis of microtubule-interfering halogenated Noscapine analogs that perturb mitosis in cancer cells followed by cell death.* Biochemical Pharmacology, 72 pp 415-426. 2006b.
[20] Thanikaivelan, P., Subramanian, V., Rao, J.R. & Nair, B.U. *Application of quantum chemical descriptor in quantitative structure activity and structure property relationship.* Chem Phys Lett, 323 pp 59–70. 2000.
[21] Naik, P.K., Alam, A., Malhotra, A. & Rizvi, O. *Molecular Modeling and Structure-activity relationship of the podophyllotoxin and its congeners.* J Biomol Screen, 15 pp 528-540.2010.
[22] 12. Naik, P.K., Sindhura, Y., Singh, T. & Singh, H. *Quantitative structure-activity relationship (QSAR) of the insecticides: the development of predictive in vivo insecticide activity models.* SAR QSAR in Env Res, 20 pp 551-556. 2009.
[23] Mane, J.Y., Klobukowski, M.J., Huzil, T. & Tuszynski, J. *Free Energy Calculations on the Binding of Colchicine and Its Derivatives with the α/β-Tubulin Isoforms.* J Chem Inf Model, 48 (9) pp 1824-1832. 2008.
[24] Naik, P.K., Santoshi, S., Rai, A. & Joshi, H.C. *Molecular modelling and competition binding study of Br- Noscapine and colchicine provide insight into Noscapinoid-tubulin binding site.* J Mol Graphics and Model, 29 pp 947-955. 2011.
[25] Laskowski, R.A., MacArthur, M.W., Moss, D.S. & Thornton, J.M. *PROCHECK: a program to check the stereochemical quality of protein structures.* J App Crystal, 26 pp 283-291. 1993.
[26] Ramachandran, G.N., Ramakrishnan, C. & Sasisekharan, V. *Stereochemistry of polypeptide chain configurations.* J Mol Biol, 7 pp 95–99. 1963.
[27] Colovos, C. & Yeates, T.O. *Verification of protein structures: Patterns of non-bonded atomic interactions.* Protein Sci, 2 pp 1511-1519. 1993.
[28] Eisenberg, D., Luthy, R. & Bowie, J.U. *VERIFY3D: assessment 694 of protein models with three-dimensional profiles.* Methods Enzymol, 277 pp 396–404. 1997

[29] Joshi, H.C., Salil, A., Bughani, U. & Naik, P.K. *Noscapinoids: a new class of anticancer drugs demand bio-technological intervention,* Medicinal Plant Biotechnology, Ed Arora R CAB e-Books CABI (H ISBN 9781845936785) .2010.
[30] Mahmoudian, M. & Rahimi-Moghaddam, P. *The anti-cancer activity of Noscapine: A review*. Recent Pat Anticancer Drug Discov, 4(1) pp 92-97. 2009.
[31] Zhou, J., Gupta, K., Aggarwal, S., Aneja, R., Chandra, R., Panda, D. & Joshi, H.C. *Brominated derivatives of Noscapine are potent microtubule-interfering agents that perturb mitosis and inhibit cell proliferation.* Mol Pharmacol, 63 pp 799-807. 2003.
[32] Manchukonda, N.K., Naik, P.K., Santoshi, S., Lopus, M., Joseph, S., Sridhar, B. & Kantevari, S. *Rational Design Synthesis and Biological Evaluation of Third Generation α-Noscapine Analogues as Potent Tubulin Binding Anti-Cancer Agents.* PLOS ONE, 8(10) pp 77970. 2013.
[33] Naik, P.K., Chatterji, B.P., Vangapandu, S.N., Aneja, R., Chandra, R., Kanteveri, S. & Joshi, H.C. *Rational design synthesis and biological evaluations of amino-Noscapine: A high affinity tubulin-binding Noscapinoids*. J Comput Aided Drug Design, 25 pp 443-454. 2011.
[34] Friesner, R.A., Banks, J.L., Murphy, R.B., Halgren, T.A., Klicic, J.J., Mainz, D.T., Repasky, M.P., Knoll, E.H., Shelley, M., Perry, J.K., Shaw, D.E., Francis, P. & Shenkin, P.S. *Glide: a new approach for rapid accurate docking and scoring 1 method and assessment of docking accuracy.* J Med Chem, 47 pp 1739–1749. 2004.
[35] Halgren, T.A., Murphy, R.B., Friesner, R.A., Beard, H.S., Frye, L.L., Pollard, W.T. & Banks, J.L. *Glide: a new approach for rapid accurate docking and scoring 2 Enrichment factors in database screening.* J Med Chem, 47 pp 1750-1759. 2004.
[36] Wang, Y., Sparano, J.A., Fineberg, S., Stead, L., Sunkara, J., Horwitz, S.B. & McDaid, H.M. *High Expression of Class III β-Tubulin Predicts Good Response to Neoadjuvant Taxane and Doxorubicin/Cyclophosphamide-Based Chemotherapy in Estrogen Receptor–Negative Breast Cancer.* Clin Breast Cancer, 13(2) pp 103–108. 2013.
[37] Mozzetti, S., Ferlini, C., Concolino, P. et al. *Class III B-Tubulin Overexpression Is a Prominent Mechanism of Paclitaxel Resistance in Ovarian Cancer Patients.* Clin Cancer Res, 11 pp 298-305. 2005.
[38] Joshua. A., McCarroll, Gan P.P., Liu, M. & Kavallaris, M. *βIII-Tubulin Is a Multifunctional Protein Involved in Drug Sensitivity and Tumorigenesis in Non–Small Cell Lung Cancer.* Clin Cancer Res, 70(12) pp 4995-5003. 2010.
[39] Nicoletti, M.I., Valoti, G., Giannakakou, P. et al. *Expression of β_Tubulin Isotypes in Human Ovarian Carcinoma Xenografts and in a Sub-Panel of Human Cancer Cell Lines from the NCI-Anticancer Drug Screen: Correlation with Sensitivity to Microtubule Active Agents.* Clin Cancer Res, 7 pp 2912 – 2922. 2001.
[40] Se`ve, P., Issac, S. Tr`edan, O. et al. *Expression of Class III B-Tubulin Is Predictive of Patient Outcome in PatientswithNon Small Cell Lung Cancer Receiving Vinorelbine-Based Chemotherapy*. Clin Cancer Res, 11 pp 5481 – 5486. 2005.
[41] Zhang, Y., Yang, H., Liu, J. et al. *High expression levels of class III β-tubulin in resected non-small cell lung cancer patients are predictive of improved patient survival after vinorelbine-based adjuvant chemotherapy.* Oncology letters, 6 pp 220 – 226. 2013.
[42] Kim, Y.S., Tseng, C.Y., Mane, J.Y., Winter, P., Johnson, L., Huzil, T., Izbicka, E., Luduena, R.F. & Tuszynski, J. *Quantitative analysis of the effect of tubulin isotype expression on sensitivity of cancer cell lines to a set of novel colchicine derivatives.* Molecular Cancer, 9 pp 131. 2010.
[43] Case, D.A., Walker, R.C. et al. *AMBER 11 University of California SanFrancisco* .2010.
[44] Srinivasan, J., Cheatham, T.E., Cieplak, P., Kollman, P.A. & Case, D.A. *Continuum Solvent Studies of the Stability of DNA RNA and Phosphoramidate−DNA Helicesm.* J Am Chem Soc, 120 pp 9401–9409. 1998.

[45] Kollman, P.A., Massova, I., Reyes, C., Kuhn, B., Huo, S., Chong, L., Lee, M., Lee, T., Duan, Y., Wang, W., Donini, O., Cieplak, P., Srinivasan, J., Case, D.A. & Cheatham, T.E. *Calculating structures and free energies of complex molecules: combining molecular mechanics and continuum models.* Acc Chem Res, 33 pp 889-97. 2000.

[46] Zhou R, Frienser RA, Ghosh A, Rizzo RC, Jorgensen WL, Levy RM (2001) New linear interaction method for binding affinity calculations using a continuum solvent model. J PhysChem B 105:10388–10397.

[47] Hota SK, Barhwal K, Ray K, Singh SB, Ilavazhagan G. Ceftriaxone rescues hippocampal neurons from excitotoxicity and enhances memory retrieval in chronic hypobaric hypoxia. Neurobiology of Learning and Memory. 2008;89:522-32.

[48] Hota SK, Hota KB, Prasad D, Ilavazhagan G, Singh SB. Oxidative-stress-induced alterations in Sp factors mediate transcriptional regulation of the NR1 subunit in hippocampus during hypoxia. Free Radical Biology & Medicine. 2010;49:178-91.

LIST OF PUBLICATIONS

1. **Seneha Santoshi,** Pradeep K. Naik and Harish C. Joshi (2011). Rational design of novel anti-microtubule agent (9-azido-noscapine) from quantitative structure activity relationship (QSAR) evaluation of noscapinoids. *Journal of Biomolecular Screening* **.** 16(9):1047-1058. [ISSN: 1087-0571, **IF: 2.207]**

2. **Seneha Santoshi** and Pradeep K. Naik (April 2014). Molecular insight of isotypes specific β-tubulin interaction of tubulin heterodimer with noscapinoids. *Journal of computer aided Molecular design* (Revision submitted) [ISSN: 0920-654X**, IF: 3.172]**

3. **Seneha Santoshi** and Pradeep K. Naik (2012).Evaluation of structure activity relationship of Noscapinoids utilizing field based 3D QSAR modeling. *International Journal of Fundamental and Applied Sciencces.* 1: 481-87.[ISSN: 2278-1404]

4. **Seneha Santoshi,** Naresh Kumar Manchukonda, Manu Lopus, Silja Joseph, Charu Suri, Sunil K Hota, Saroj K Das, Srinivas Kantevari and Pradeep Kumar Naik (2014). Computer aided design and chemical synthesis of microtubule-interfering Suzuki derivatives of noscapine that perturb mitosis in cancer cells followed by cell death. (communicated to *Journal of Biomolecular Structure and Dynamics* **[IF:4.9]**

CONFERENCE PRESENTATIONS

1. **Seneha Santoshi** and Pradeep K. Naik. A three dimensional QSAR model building utilizing structural determinants of noscapine derivatives for tubulin binding affinity prediction. **Poster presented** in International conference on "biotechnology advances :omics approaches and way forward (ICBA-2012)"organized by centre of biotechnology (supported by DST-FIST, govt. of India) Siksha 'o' Anusandhan University, Bhubaneswar 20 -22 December, 2012.)